Suppl. References

1. Suzuki A, Sanda N, Miyawaki Y, et al. Down-regulation of PROS1 Gene Expression by 17beta-Estradiol via Estrogen Receptoralpha (ERalpha)-Sp1 Interaction Recruiting Receptor-interacting Protein 140 and the Corepressor-HDAC3 Complex. J Biol Chem 2010;285:13444-53.
2. Chen Z, Pelc LA, Di Cera E. Crystal structure of prethrombin-1. Proc Natl Acad Sci 2010;107:19278-83.
3. Li W, Johnson DJD, Esmon CT, Huntington JA. Structure of the antithrombin-thrombin-heparin ternary complex reveals the antithrombotic mechanism of heparin. Nat Struct Mol Biol 2004;11:857-62.

Oncogene (2012) **31,** 4667–4676

www.nature.com/onc

ORIGINAL ARTICLE

Aberrant activation of ALK kinase by a novel truncated form ALK protein in neuroblastoma

J Okubo[1], J Takita[1,2], Y Chen[1], K Oki[1], R Nishimura[1], M Kato[1], M Sanada[3], M Hiwatari[1], Y Hayashi[4], T Igarashi[1] and S Ogawa[3]

Anaplastic lymphoma kinase (ALK) was originally identified from a rare subtype of non-Hodgkin's lymphomas carrying t(2;5)(p23;q35) translocation, where ALK was constitutively activated as a result of a fusion with nucleophosmin (NPM). Aberrant ALK fusion proteins were also generated in inflammatory fibrosarcoma and a subset of non-small-cell lung cancers, and these proteins are implicated in their pathogenesis. Recently, ALK has been demonstrated to be constitutively activated by gene mutations and/or amplifications in sporadic as well as familial cases of neuroblastoma. Here we describe another mechanism of aberrant ALK activation observed in a neuroblastoma-derived cell line (NB-1), in which a short-form ALK protein ($ALK^{del2\text{-}3}$) having a truncated extracellular domain is overexpressed because of amplification of an abnormal *ALK* gene that lacks exons 2 and 3. $ALK^{del2\text{-}3}$ was autophosphorylated in NB-1 cells as well as in $ALK^{del2\text{-}3}$-transduced cells and exhibited enhanced *in vitro* kinase activity compared with the wild-type kinase. $ALK^{del2\text{-}3}$-transduced NIH3T3 cells exhibited increased colony-forming capacity in soft agar and tumorigenicity in nude mice. RNAi-mediated ALK knockdown resulted in the growth suppression of $ALK^{del2\text{-}3}$-expressing cells, arguing for the oncogenic role of this mutant. Our findings provide a novel insight into the mechanism of deregulation of the ALK kinase and its roles in neuroblastoma pathogenesis.

Oncogene (2012) **31,** 4667–4676; doi:10.1038/onc.2011.616; published online 16 January 2012

Keywords: neuroblastoma; *ALK*; truncated form ALK; amplification

INTRODUCTION

Anaplastic lymphoma kinase (ALK) (OMIM: 105590) is an orphan receptor tyrosine kinase (RTK) that was initially characterized as a fusion partner of the nucleophosmin (NPM)-ALK chimeric protein associated with the t(2;5)(p23;q35) translocation in anaplastic large-cell lymphoma.[1,2] Subsequent studies have revealed that various ALK-containing fusion proteins with different fusion partners are generated in various solid tumors, such as inflammatory myofibroblastic tumors, non-small-cell lung cancer and squamous cell carcinoma of the esophagus.[3–6] Furthermore, recent genome-wide studies have revealed that *ALK* is activated by gene amplification and nucleotide mutations and is involved in the pathogenesis of both familial and sporadic neuroblastoma.[7–10]

Neuroblastoma is an intractable, solid tumor of childhood arising from the neural crest and can arise anywhere along the sympathetic nervous system.[11] The overall 5-year survival rate for neuroblastoma is $\leqslant$40%, despite current intensive multimodality treatments.[12–14] Considering that *ALK* mutations preferentially involve advanced neuroblastoma with a poor outcome, the more relevant implication of these findings is that ALK inhibitors may improve the clinical outcome of children suffering from intractable neuroblastoma.

In this study, we demonstrated another mechanism of aberrant ALK activation in neuroblastoma, in which an abnormal *ALK* gene with a deletion of exons 2 and 3 was amplified in a neuroblastoma-derived cell line (NB-1), leading to high-level expression of an ALK protein variant with a truncated extracellular domain ($ALK^{del2\text{-}3}$). Furthermore, we demonstrated that $ALK^{del2\text{-}3}$ had constitutive kinase activity and showed a transforming capacity in NIH3T3 cells. Moreover, ALK inhibition experiments using small interfering RNA (siRNA)-mediated gene knockdown and the low-molecular-weight compound, TAE684, also supported the oncogenic role of $ALK^{del2\text{-}3}$. Our results will help elucidate the mechanism of aberrant activation of ALK kinase and the role of activated ALK in the pathogenesis of neuroblastoma.

RESULTS

Detection of a short-form ALK protein in NB-1 cells

To examine the status of ALK in neuroblastoma, western blotting analysis was performed with a panel of 24 neuroblastoma-derived cell lines (Table 1). Among the 24 samples examined, the NB-1 cell line showed high-level expression of an ALK protein having a low molecular weight of 208 kDa compared with the molecular weight of 220 kDa for the wild-type protein (Figure 1a). Subsequent sequencing and reverse transcription–polymerase chain reaction (RT–PCR) analysis of *ALK* messages from NB-1 cells revealed the presence of an aberrant *ALK* transcript with a 285-bp in-frame deletion in the 5′ region corresponding to exons 2 and 3 (Figures 1b and c), which should result in the production of an abnormal ALK protein with a truncated N-terminal extracellular domain. Using a primer set for exons 2 and 3, a 166-bp product was also detected in NB-1 cells, indicating the presence of the wild-type *ALK* allele in NB-1 cells (Figures 1b and c). The deletion spanned 224–318 amino acids (aa), including the N-terminal end of the first meprin A5 protein and receptor protein tyrosine phosphatase mu (MAM) domain (aa 264–427) (Figure 1d).[15,16] We analyzed full-length *ALK* cDNAs isolated from 71 primary neuroblastoma samples for possible nucleotide deletions using RT–PCR (Table 2), but no deletions were detected.

[1]Department of Pediatrics, Graduate School of Medicine, University of Tokyo, Tokyo, Japan; [2]Department of Cell Therapy and Transplantation Medicine, Graduate School of Medicine, University of Tokyo, Tokyo, Japan; [3]Cancer Genomics Project, Graduate School of Medicine, University of Tokyo, Tokyo, Japan and [4]Gunma Children's Medical Center, Maebashi, Japan. Correspondence: Dr J Takita, Cell Therapy and Transplantation Medicine, Graduate School of Medicine, University of Tokyo, 7-3-1, Hongo, Bunkyo-ku, Tokyo 113-8655, Japan. E-mail: jtakita-tky@umin.ac.jp
Received 22 May 2011; revised and accepted 29 November 2011; published online 16 January 2012

Table 1. Neuroblastoma cell lines used in this study

Cell line	*MYCN amplification*	*ALK status*
CHP-134	–	WT
GOTO	+	WT
LAN-1	+	F1174L
LAN-2	+	WT
LAN-5	+	R1275Q
NB-1	–	Amplification
NB-16	+	WT
NB-19	+	WT
NB-69	–	WT
NH-12	+	WT
SCMC-N2	+	F1174L
SCMC-N4	+	WT
SCMC-N5	+	K1062M
SJNB-1	–	WT
SJNB-2	+	R1275Q
SJNB-3	–	WT
SJNB-4	+	F1174L
SJNB-5	+	WT
SJNB-6	+	WT
SJNB-7	+	WT
SJNB-8	+	WT
SK-N-SH	–	F1174L
TGW	+	R1275Q
UTP-N-1	+	WT

Abbreviations: ALK, anaplastic lymphoma kinase; WT, wild type.

Structural abnormality of the *ALK* gene in NB-1 cells

As reported previously,[7] our single-nucleotide polymorphism array-based copy number analysis of NB-1 cells disclosed high-level gene amplification of the *ALK*-containing 2p24 segment. This should explain the high *ALK* expression observed in this cell line (Figures 1a and b). In particular, the genomic copy numbers within the 2p23 amplicon exhibited a transient decrease at three consecutive single-nucleotide polymorphisms (Chr2: 29 911 541–29 912 210), which corresponded to *ALK* intron 3, raising the possibility that a gene deletion involving exons 2 and 3 was responsible for the aberrant *ALK* transcript (Figure 2a). To confirm this, we performed Southern blot analysis of NB-1 genomic DNA using fragments exons 1–4 as probes (Figure 2b). As shown in Figures 2c–e, Southern blot analysis confirmed *ALK* gene amplification in NB-1 cells, as these blots showed high-intensity signals for each of the four *ALK*-specific probes in NB-1 cells compared with those in the controls. However, a significant difference was observed in the signal intensity between the fragments containing exons 1/4 and exons 2/3 in the NB-1 lanes, in which exons 1 and 4 showed 3.9- and 3.8-fold higher signals than exons 2 and 3, respectively. This result was confirmed by quantitative genomic PCR analysis using seven primer sets located within *ALK* exons 1–4 (Figure 2f). Taken together, these results indicate that the 2p23 amplicons were heterogeneous with regard to the species of *ALK* it contained, among which the predominant *ALK* allele had a deletion at exons 2 and 3, and these amplicons were responsible for the generation of $ALK^{del2\text{-}3}$.

Oncogenic potential of an aberrant short-form ALK protein

We next evaluated the oncogenic role of the truncated form of ALK found in NB-1 cells in terms of its kinase activity. As shown in Figure 3a, $ALK^{del2\text{-}3}$ was strongly phosphorylated in NB-1 cells, whereas the wild-type ALK expressed in NH-12 cells was unphosphorylated. Similar to the constitutive active F1174L ALK mutant when expressed in NIH3T3 cells, $ALK^{del2\text{-}3}$ had enhanced ALK phosphorylation compared with wild-type ALK (Figure 3b). Moreover, after anti-FLAG immunoprecipitation of FLAG-tagged ALK constructs, $ALK^{del2\text{-}3}$ and F1174L ALK mutants were strongly phosphorylated according to western blot analysis using a PY20 blot (Figure 3c). In addition, they exhibited enhanced kinase activity in an *in vitro* kinase assay using the YFF peptide as a substrate (Figure 3d). To confirm kinase activity of the $ALK^{del2\text{-}3}$ mutant, we further examined *in vitro* kinase activities of wild-type and mutant ALK-expressing NIH3T3 cells using a universal substrate. The immunoprecipitated FLAG-tagged $ALK^{del2\text{-}3}$ mutant showed significantly increased kinase activity (Supplementary Figure S1).

In an analysis of activated downstream signaling, significantly enhanced STAT3 phosphorylation was observed in $ALK^{del2\text{-}3}$ and F1174L mutants, whereas a significant increase in AKT phosphorylation was not detected in any samples (Figure 3e and Supplementary Figure S2). Extracellular regulated kinase (ERK) was probably phosphorylated in the F1174L mutant and wild-type ALK, but not in $ALK^{del2\text{-}3}$ (Figure 3e). The results of three independent experiments were quantified by densitometric scanning (Supplementary Figure S2).

We investigated the oncogenic potential of the $ALK^{del2\text{-}3}$ mutant in NIH3T3 cells, in terms of colony formation in soft agar and tumor generation in nude mice. As shown in Figures 4a and b, NIH3T3 cells that were stably transduced with $ALK^{del2\text{-}3}$ and ALK^{F1174L} produced a significantly higher numbers of colonies in soft agar than mock or wild-type *ALK*-transduced cells (Figures 4a and b). When inoculated into nude mice, the $ALK^{del2\text{-}3}$-transduced NIH3T3 cells invariably developed into subcutaneous tumors (5/5), whereas the mock and wild-type *ALK*-transfected cells did not develop into tumors (0/5) (Figure 4c).

$ALK^{del2\text{-}3}$ was retained in the endoplasmic reticulum

Among ALK signaling pathway molecules, STAT3 was only strongly phosphorylated by $ALK^{del2\text{-}3}$, suggesting that the $ALK^{del2\text{-}3}$ mutant was exclusively involved in the STAT3 pathway. It has been previously reported that intracellular fms-like tyrosine kinase-internal tandem duplication activation induces an aberrant downstream signaling outcome.[17] To determine whether $ALK^{del2\text{-}3}$ expresses at the cell surface and mediates signals from endoplasmic reticulum (ER), we analyzed localization and deglycosidation of $ALK^{del2\text{-}3}$ in NB-1 cells and wild-type ALK in NH-12 cells. Immunofluorescence staining revealed that ALK in NB-1 cells was almost colocalized with PDI, whereas ALK in NH-12 cells was largely located at the plasma membrane (Figure 5a). As shown in Supplementary Figure S4, colocalization of ALK and PDI was quantified using the Pearson's correlation coefficient. Moreover, to determine whether $ALK^{del2\text{-}3}$ was subjected to maturation of its oligosaccharides, we examined the endoglycosidase H sensitivity of ALK expressed in NB-1 and NH-12 cells. As shown in Figure 5b, $ALK^{del2\text{-}3}$ in NB-1 cells revealed the high sensitivity of endoglycosidase H compared with the wild-type ALK in NH-12 cells, suggesting that intercellular localization of $ALK^{del2\text{-}3}$ was associated with a defect in N-linked glycosylation.[18] These results indicate that $ALK^{del2\text{-}3}$ is mainly located at ER and aberrantly activates the STAT3 pathway from there.

Effect of ALK inhibition on cell growth in NB-1 cells

Finally, we examined the effect of ALK inhibition on NB-1 cell proliferation using the small-molecule ALK inhibitor TAE684 and siRNA-mediated ALK knockdown. NB-1 cell growth was effectively inhibited by TAE684 with a half maximal inhibitory concentration (IC_{50}) of 13 nM, which was similar to the IC_{50} for SK-N-SH (49 nM; an *ALK*-mutated TAE684-sensitive neuroblastoma cell line), but substantially lower than the IC_{50} for TGW cells with the ALK^{R1275Q} mutant (310 nM), the glioblastoma-derived cell line H4 with wild-type ALK (190 nM) and NIH3T3 cells with no ALK expression (380 nM) (Figure 6a). Similarly, siRNA-mediated knockdown of $ALK^{del2\text{-}3}$ in NB-1 cells resulted in significant suppression of cell proliferation compared with controls transfected with nonspecific

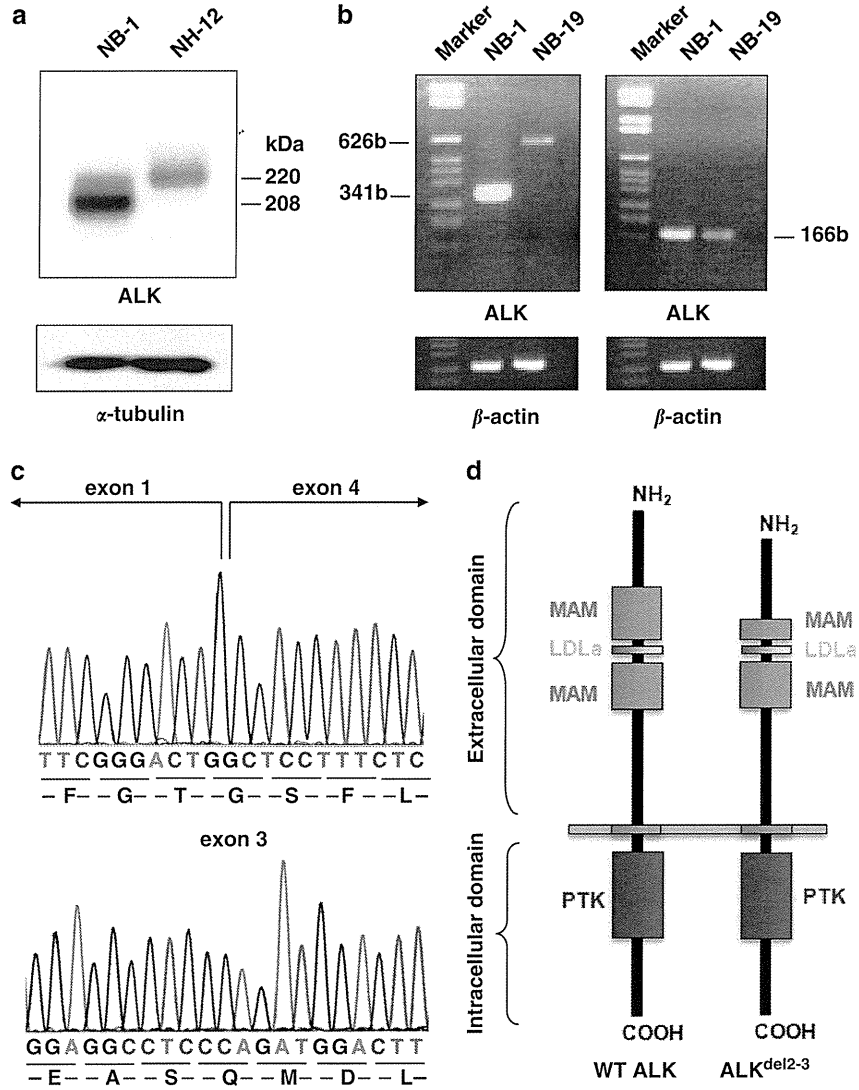

Figure 1. Detection of an aberrant truncated form of ALK in NB-1 cells. (**a**) Western blot analysis of ALK in neuroblastoma-derived cell lines. NB-1 cells strongly expressed the truncated form with a molecular mass of 208 kDa. In contrast, wild-type ALK-expressing neuroblastoma-derived cell lines (NH-12) revealed an ALK protein with a molecular mass of 220 kDa. α-Tubulin staining as loading control. (**b**) RT-PCR analysis of *ALK* exons 1-5 and exons 2 and 3 in the neuroblastoma cell lines. A short PCR product with 314 bp was detected in NB-1 cells, whereas much longer PCR products with 627 bp were detected in NB-19 cells with wild-type *ALK*. Wild-type *ALK* was detected in both NB-1 and NB-19 cells using *ALK* exon 2 and 3 primers. (**c**) Subsequent sequence analysis of *ALK* cDNA from NB-1. In-frame deletion in exons 2 and 3 was confirmed by direct sequencing. Sequencing of the PCR product detected by RT-PCR for *ALK* exons 2 and 3 confirmed the presence of wild-type *ALK* in NB-1 cells. Lower panel represents DNA sequencing for *ALK* exon 3 in NB-1 cells. (**d**) Schematic representation of the truncated form of aberrant ALK. The extracellular domain of ALK comprises two MAM domains (aa 264-427 and 480-626), one low-density lipoprotein class A (LDLa) motif (aa 453-471) and a glycine-rich region (aa 816-940) (Palmer *et al.*[30]). Because exons 2 and 3 of *ALK* implicate 224-318 aa, the in-frame deleted mutant led to a translational truncated form of the first MAM domain. PTK, protein tyrosine kinase.

siRNA, but the suppression apparently decreased in wild-type ALK-expressing NH-12 cells (Figures 6b and c). As shown in Supplementary Figure S3, significant inhibition was observed in NB-1 cells with ALK knockdown compared with that in the negative control ($P<0.05$, Mann-Whitney *U*-test).

DISCUSSION

Deregulated activation of ALK has been implicated in various human cancers through either generation of fusion proteins, overexpression or single amino-acid changes. In this study, we described a novel mechanism of oncogenic activation of *ALK* that operated in a neuroblastoma-derived cell line, NB-1. In NB-1 cells, an aberrant form of *ALK* that lacks exons 2 and 3 was amplified, leading to high-level expression of an N-terminal-truncated kinase, ALK^{del2-3}, and our functional studies confirmed the oncogenic role of ALK^{del2-3}. First, ALK^{del2-3} underwent autophosphorylation in NB-1 and NIH3T3 cells and demonstrated enhanced kinase activity, promoting downstream signaling pathways such as the STAT3 pathway. Second, ALK^{del2-3} promoted colony formation in soft agar and tumorigenicity when transduced into NIH3T3 cells in nude mice. Finally, inhibition of cell growth was observed when we treated NB-1 cells with TAE684, an ALK-specific kinase inhibitor, and siRNA-mediated gene knockdown. Unfortunately, screening of 71 primary neuroblastoma specimens and 23 neuroblastoma-derived cell lines did not identify a similar mechanism of ALK oncogenic activation in neuroblastoma; therefore, it is not a common mechanism for ALK activation in

Table 2. Neuroblastoma fresh tumor samples used in this study

Clinicopathological findings	*Samples*
Age (years)	
>1	41
<1	30
Stage	
1	16
2	11
3	12
4	29
4S	2
ND	1
MYCN status	
Amplification (+)	11
(−)	58
ND	2
ALK status	
Amplification	1
Mutation	6
Wild type	64
Total	71

Abbreviations: ALK, anaplastic lymphoma kinase; ND, not determined.

neuroblastoma. Nevertheless, the discovery of this unique ALK form will add to our knowledge with regard to the pathogenesis of neuroblastoma and will help to elucidate the mechanism of ALK activation.

Abnormal activation of RTK through a deletion in its extracellular domain has been documented in several cancers.[19-21] A common example of abnormal RTK activation is the epidermal growth factor receptor class III variant, which is present in a substantial proportion of malignant gliomas and other human cancers, but completely absent in normal tissues.[22,23] This variant results from a transcript having an 801-bp in-frame deletion of EGFR that corresponds to exons 2–7, which leads to the generation of a protein with a truncated extracellular domain.[21,24] Several molecular mechanisms have been implicated in the oncogenic pathway with epidermal growth factor receptor class III variant downstream signaling.[21,24] For example, in addition to ligand-independent self-dimerization, epidermal growth factor receptor class III variant has been shown to constitutively interact with adaptor proteins SHC and GRB2, which are involved in the recruitment of the RAS pathway.[25] The recepteur d'origine nantais (RON) RTK variant with a deletion in the first immunoglobulin-plexin transcription domain (RONΔ160) has also been considered as a constitutively activated kinase in several human cancers.[20,26] RON belongs to the MET proto-oncogene family, which plays a critical role in epithelial cell homeostasis and tumorigenic development.[27] RONΔ160 is derived from a *RON* mRNA transcript by alternative splicing that eliminates 109 aa residues from the extracellular domain of RON β-chain and is expressed in >50% of primary colon cancers and 90% of brain tumors, but not in any normal tissues.[26,28] The deleted 109 aa residues are encoded by exons 5/6, which constitute the first immunoglobulin-plexin transcription domain in the RON β-chain.[26,28] The mechanism for the oncogenic activation of RONΔ160 is believed to be one in which the deletion in the extracellular domain causes conformational changes in the kinase and leads to spontaneous dimerization, which in turn causes constitutive receptor phosphorylation and increased intracellular signaling activation.[26,28,29]

The ALK^{del2-3} variant consists of a 282-bp in-frame deletion of *ALK* that corresponds to 224–318 aa in the first MAM domain (Figure 1d). ALK is the sole RTK that contains MAM domains in its extracellular region.[30] Although MAM domains are thought to participate in cell–cell interactions, their significance in ALK function remains unclear.[15,16] Thus, the functional significance of MAM deletion in the truncated ALK is still elusive. As the deleted region of *ALK* detected in NB-1 cells is in close proximity to a ligand-binding domain (391–401 aa), this deletion may structurally alter the ligand-binding domain. Similar to epidermal growth factor receptor class III variant and RONΔ160, the ALK^{del2-3} variant may be constitutively activated in a ligand-independent manner and/or through spontaneous dimerization, although the exact mechanism of constitutive activation of ALK^{del2-3} is yet to be elucidated.

Oncogenic ALK transformation is mediated by interactions with downstream molecules that trigger a substantial intercellular signaling cascade.[31] The most relevant and best-characterized ALK downstream pathways are the RAS-ERK, JAK3-STAT3 and PI3K-AKT pathways.[31] Among ALK signaling molecules, STAT3 is only strongly phosphorylated by ALK^{del2-3}, suggesting that besides F1174L or K1062M ALK mutants,[7] ALK^{del2-3} would be exclusively involved in the STAT3 pathway. Recently, it has been reported that the oncogenic mutant of fms-like tyrosine kinase-internal tandem duplication aberrantly activates STAT5 when localized at ER, but fails to activate MAPK and AKT signaling.[17] Thus, this raises the possibility that involvement of the STAT3 pathway in ALK^{del2-3}-expressing cells resembles the fms-like tyrosine kinase-internal tandem duplication mutant.[17] Immunofluorescence staining and the endoglycosidase H sensitivity assay revealed that ALK^{del2-3} is mainly located at ER and aberrantly activates the STAT3 pathway from ER. Taken together, our results suggest that intracellular activation of ALK^{del2-3} switches downstream signaling to the ALK pathway.[18]

Furthermore, ERK phosphorylation was similarly elevated in cells expressing wild-type or F1174L ALK. This may have been because of enhanced expression of exogenous wild-type *ALK* by retrovirus-mediated gene transfer. Schulte *et al.*[32] reported that the high level of wild-type ALK and mutant ALK expression has similar effects on the neuroblastoma biological phenotype, which may be related to tumor growth. Taken together, the results from our study and from the study by Schulte *et al.*[32] suggest that in addition to the ALK mutants, elevated wild-type ALK expression also mediates similar molecular functions that contribute to the malignant phenotype in neuroblastoma.

In summary, we found that an N-terminal-truncated ALK protein observed in a neuroblastoma-derived cell line (NB-1) is a novel oncogenic isoform of ALK. This study provides a better understanding of the molecular mechanism of pathogenesis of neuroblastoma as well as oncogenic roles of ALK pathway.

MATERIALS AND METHODS

Specimens

In all, 24 neuroblastoma cell lines were used in this study (Table 1). The SCMC-N series was established in our laboratory.[33] The SJNB series and UTP-N-1 cells were provided by Dr AT Look and Dr A Inoue, respectively. Other cell lines were obtained from the Japanese Cancer Resource Cell Bank (http://cellbank.nibio.go.jp/wwwjcrbj.htm). All cells were maintained in RPMI 1640 medium (Gibco, Grand Island, NY, USA) supplemented with 10% fetal bovine serum in a humidified atmosphere containing 5% CO_2 at 37 °C. Primary neuroblastoma specimens were obtained through surgery or biopsy from patients who were diagnosed with neuroblastoma and who were admitted to Tokyo University Hospital, Saitama Children's Medical Center or various other hospitals between November 1993 and October 2006. The patients were staged according to the International Neuroblastoma Staging System,[34] and the clinicopathological findings are listed in Table 2.

ALK expression analyses

Total cellular proteins were resolved on a 5–10% gradient sodium dodecyl sulfate-polyacrylamide gel and electrophoretically transferred onto

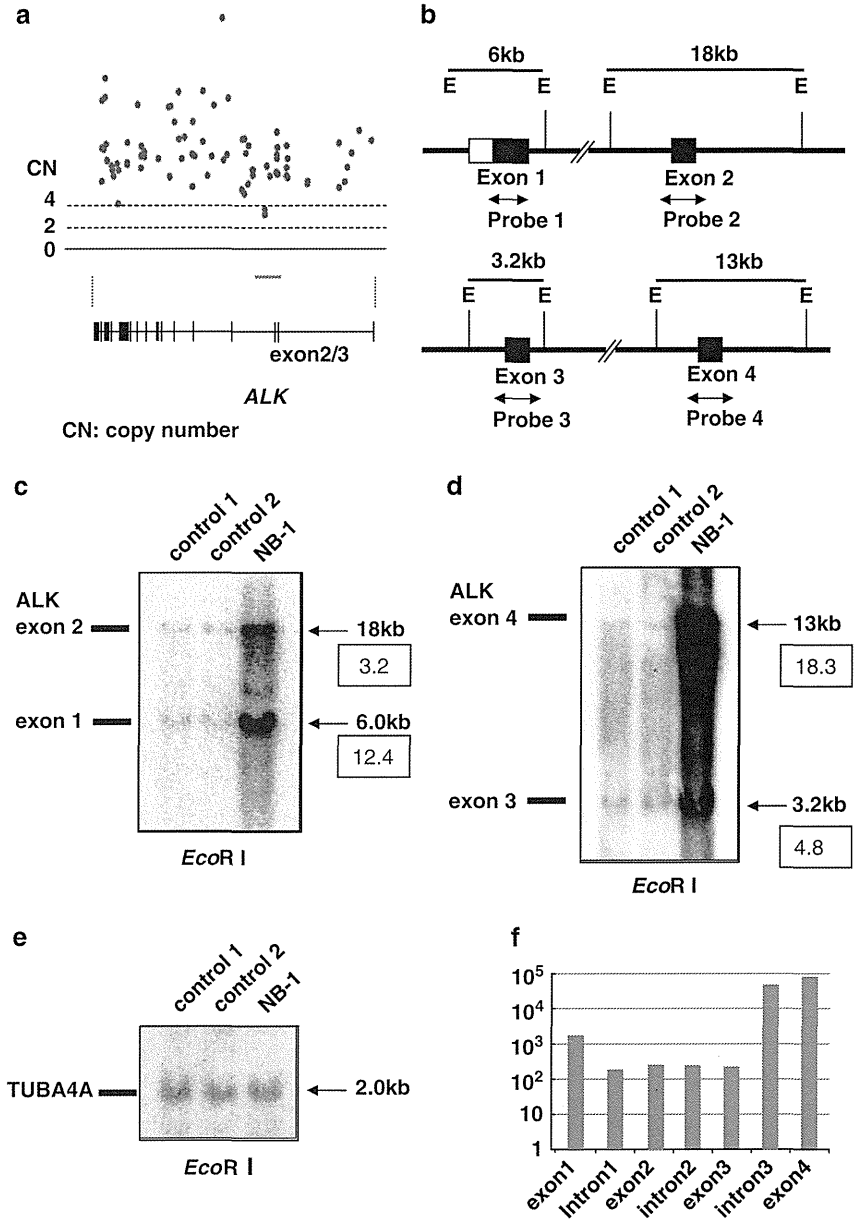

Figure 2. Genetic characteristics of the N-terminal-truncated form of ALK. (**a**) High-grade amplification of the *ALK* locus detected in NB-1 cells by single-nucleotide polymorphism array analysis (Affymetrix GeneChip 250k *Nspl*). Among the single-nucleotide polymorphism probes located within the *ALK* amplicon, three consecutive single-nucleotide polymorphism probes (Chr2: 29 911 541 and 29 912 210) located within *ALK* intron 3 showed relatively low signal intensities. The red line indicates the focal deletion within *ALK* intron 3. (**b**) Physical maps of *ALK* exons 1–4. The restriction sites and probe maps for *ALK* exons 1–4 are indicated. E: *EcoR*1. Arrows indicate probe positions. (**c**, **d**) Southern blot analysis using *ALK* exon 1–4 probes (**c**: exons 1 and 2; **d**: exons 3 and 4). Normal peripheral blood DNA was used as a germline control. Densitometric analysis was performed using the ImageQuant 400 and ImageQuant TL software version 7. (**e**) The TUBA4A probe was used as a loading control. (**f**) Quantitative genomic PCR analysis of *ALK* using seven primer sets located within *ALK* exons 1–4. The signal intensities of *ALK* introns 1 and 2 and exons 2 and 3 were lower compared with those of *ALK* exons 1 and 4 in NB-1 cells.

polyvinylidene difluoride membranes. After blocking with 5% milk in Tris-buffered saline containing 0.1% Tween (10 mM Tris-HCl (pH 7.4), 150 mM NaCl and 0.1% Tween-20), membranes were incubated for 1 h with primary antibody in TBS-T, washed and incubated for 12 h with primary antibody in 3% bovine serum albumin. The membranes were then washed again and incubated with anti-rabbit immunoglobulin G at room temperature for 1 h. Subsequently, they were extensively washed, and the proteins were visualized by enhanced chemiluminescence (Millipore, Bedford, MA, USA). Total RNA was extracted from the 24 cell lines and 71 frozen stocked tumors using Isogen reagent (Nippon Gene, Osaka, Japan) according to the manufacturer's instructions; the total RNA was analyzed by RT-PCR to synthesize cDNA using the SuperScript Preamplification System for first-strand cDNA synthesis (Life Technologies Inc., Rockville, MD, USA). RT-PCR analysis for *ALK* expression was performed as described previously,[7] using the primer sets listed in Table 3. cDNA concentration was equalized using *β-actin* expression as a control.

Southern blot analysis

High-molecular-weight DNA was prepared from cells according to standard procedures using the QIAamp DNA Mini kit (Qiagen, Valencia, CA, USA) and a modification of the protocol provided by the manufacturer.

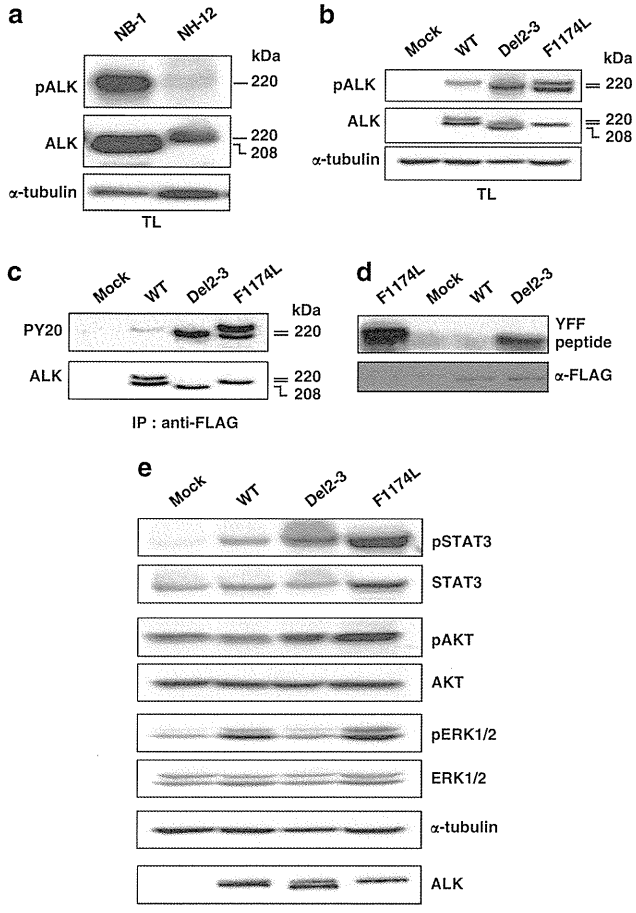

Figure 3. Kinase activities of ALK mutants and their downstream status. (**a**) Western blot analysis of ALK and phosphorylated ALK in NB-1 and NH-12 cells. NB-1 cells strongly expressed the truncated form of ALK and phosphorylated ALK compared with that in NH-12 cells. TL: Total cell lysates. (**b**) Western blot analysis of NIH3T3 cells stably expressing ALK mutants (ALK^{del2-3} and ALK^{F1174L}) and wild-type ALK. (**c**) Stably expressed ALK mutants and wild-type ALK were immunoprecipitated with an anti-FLAG antibody and subjected to western blot analysis with anti-PY20. (**d**) *In vitro* kinase assay for wild-type ALK and its mutants using the synthetic YFF peptide as a substrate. (**e**) Western blot analysis of NIH3T3 cells stably expressing ALK mutants and wild-type ALK for their downstream effectors, STAT3 (pSTAT3), AKT (pAKT) and ERK (pERK). The total amount of each molecule is also shown together with an α-tubulin blot.

DNA was extracted from NB-1 cells and peripheral normal blood cells. For Southern blot analysis, 10 μg genomic DNA was restricted with *Eco*RI and loaded onto an agarose gel.[35] After electrophoresis, the DNA was transferred to polyvinylidene difluoride membranes and hybridized with radiolabeled probes for *ALK* exons 1–4 listed in Table 3. The signal intensity of each band was quantified and calculated using the ImageQuant 400 and ImageQuant TL software version 7 (GE Healthcare, Piscataway, NJ, USA).

Quantitative genomic PCR analysis

Quantitative genomic real-time PCR was performed using SYBR Green-based quantification (Bio-Rad Laboratories, Hercules, CA, USA). The standard curve method was used to calculate the target genome numbers in the NB-1 cell line. The relative target copy number was normalized to normal human genomic DNA as a calibrator. The primer sequences used for quantitative genomic PCR are shown in Table 3.

Transforming potential of ALK mutants

ALK^{WT}-FLAG and ALK^{F1174L}-FLAG were FLAG-tagged cDNAs for wild-type *ALK* and its F1174L mutant, respectively. FLAG-tagged cDNA for the

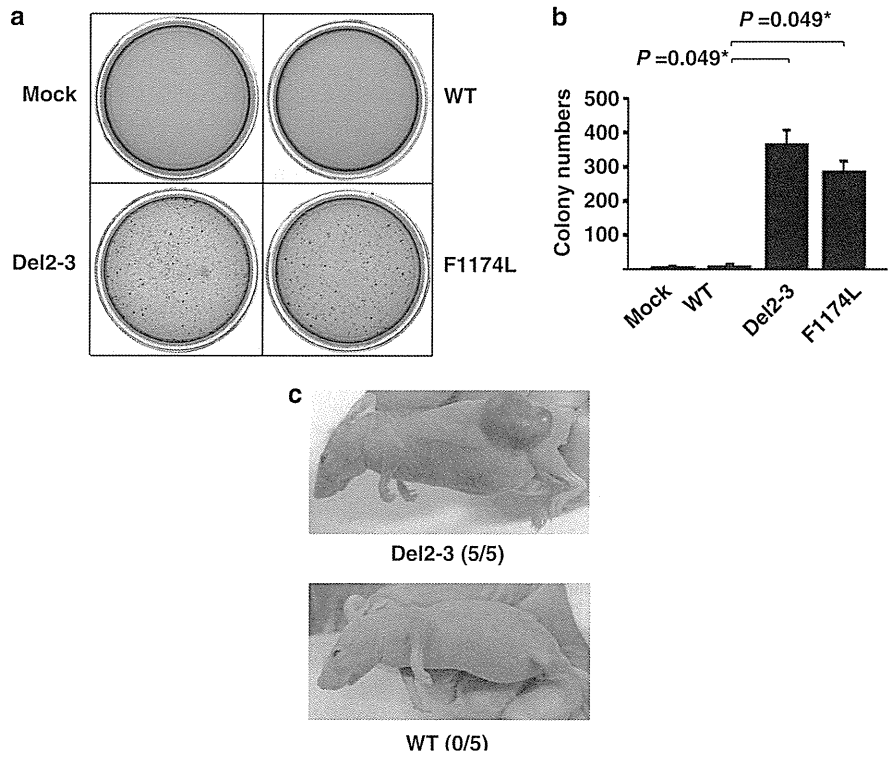

deletion mutant (*ALK*$^{del2\text{-}3}$-FLAG) was isolated from total RNA of NB-1 cells by high-fidelity PCR. After re-sequencing, each cDNA was constructed into the pcDNA3 expression plasmid and transfected into NIH3T3 cells using Effectene Transfection Reagents (Qiagen, Tokyo, Japan). Kinase assays were performed with stable clones in these constructs. For western blot analysis of mutant ALK and colony formation assays, NIH3T3 cells were stably transduced with wild-type and mutant ALK by retrovirus-mediated gene transfer. FLAG-tagged cDNA for wild-type and mutated ALK were then

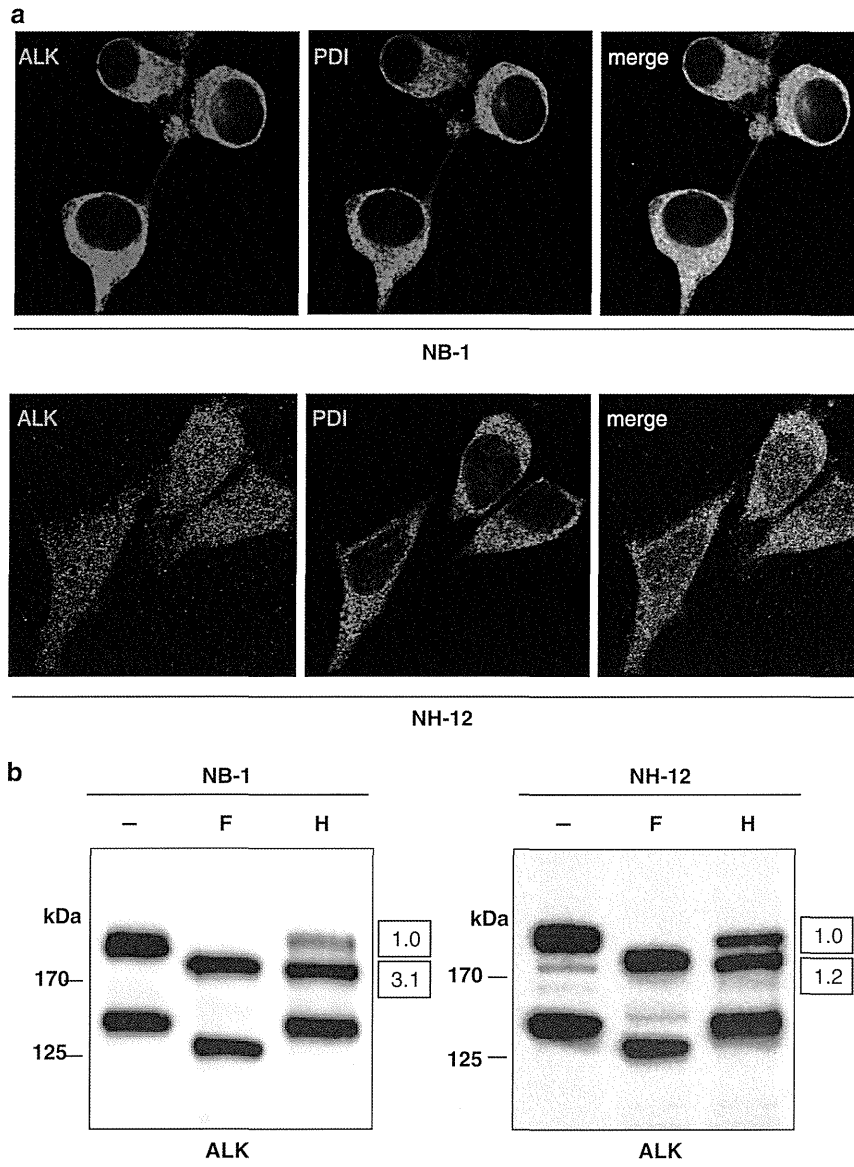

Figure 5. ER retention in the NB-1 neuroblastoma cell line and glycoprotein maturation. (**a**) Immunofluorescence confocal microscopy analysis of ALK ER localization in the neuroblastoma cell lines. The NB-1 and NH12 neuroblastoma cell lines were immunostained with the indicated antibodies and imaged using immunofluorescence microscopy to demonstrate ALK and PDI (ER-specific marker) colocalization. Cells were immunostained for ALK (red) and PDI (green), respectively. (**b**) The band of ALK$^{del2\text{-}3}$ protein of NB-1 cells is endoglycosidase H sensitive. Cell lysates from the NB-1 and NH12 neuroblastoma cell lines were incubated with N-glycosidase F (lane 2, F) and endoglycosidase H (lane 3, H). Deglycosidation profiles were compared with untreated cell lysates (lane 1). Digestion products were analyzed by western blot analysis using monoclonal anti-ALK. Signal intensities of bands in the lane endoglycosidase H were quantified by densitometric scanning using the ImageQuant 400 and ImageQuant TL software version 7. Signal intensity of approximate190 kDa band that revealed sensitivity to endoglycosidase H in NB-1 cells showed 3.1-fold higher than that of upper band.

Figure 4. Oncogenic role of the aberrant truncated form of ALK. (**a**) NIH3T3 cells stably expressing mutant kinases (ALK$^{del2\text{-}3}$ and ALK^{F1174L}) showed increased colony formation in soft agar compared with cells expressing wild-type kinase. (**b**) The average numbers of colonies in triplicate experiments are plotted. Standard deviation is indicated. Results showing significant differences compared with experiments using wild-type ALK are indicated by asterisks with *P*-values. (**c**) *In vivo* tumorigenicity assay in nude mice. Tumor formation assay in nude mice in which 1.0×10^7 NIH3T3 cells expressed wild-type ALK and the ALK$^{del2\text{-}3}$ mutant by the calcium phosphate method. Tumor formation was evaluated 21 days after inoculation.

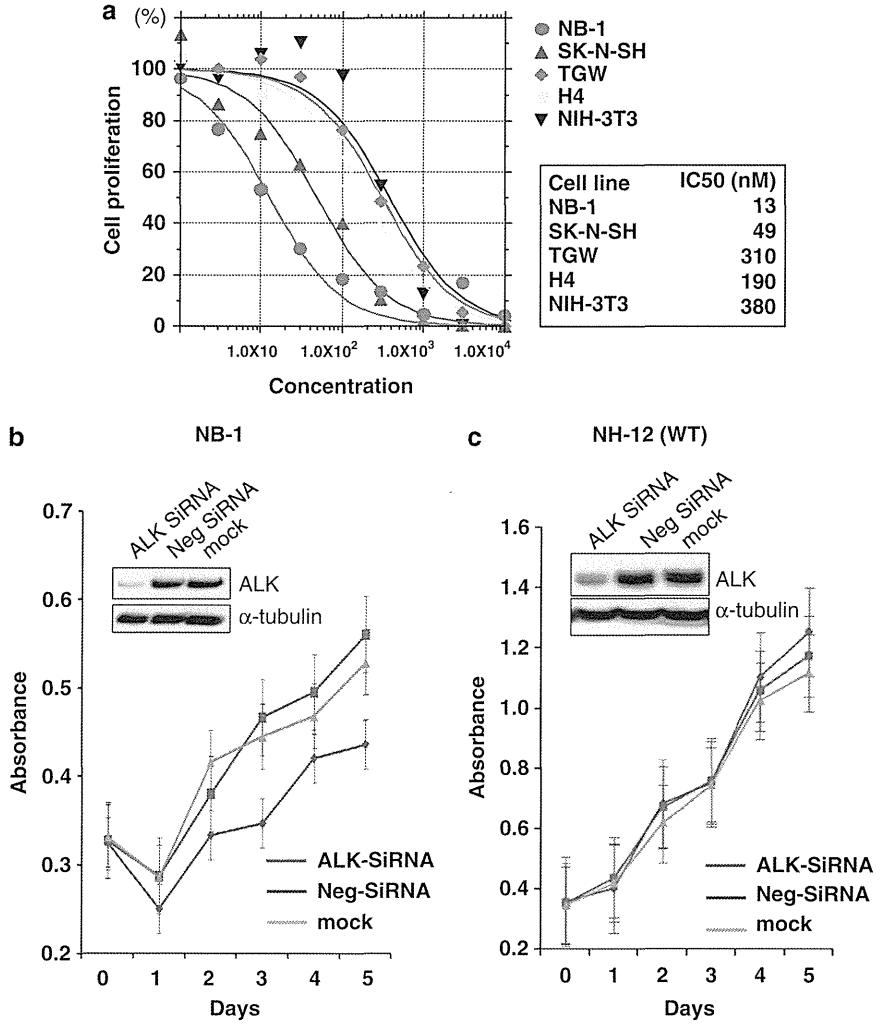

Figure 6. Effect of ALK inhibition on NB-1 cell proliferation using the ALK inhibitor TAE684 and siRNA-mediated ALK knockdown. (**a**) NB-1 cell growth was effectively inhibited by TAE684, with an IC_{50} similar to that for SK-N-SH (an *ALK*-mutated TAE684-sensitive neuroblastoma cell line), but substantially lower than that for NIH3T3 cells with no ALK expression. (**b**, **c**) Effect of RNAi-mediated ALK knockdown on cell proliferation in neuroblastoma cell lines expressing either the $ALK^{del2\text{-}3}$ mutant (NB-1) or wild-type ALK (NH-12). Cell growth was measured using the Cell Counting kit-8 after knockdown experiments using ALK-specific siRNAs, negative control siRNAs or mock experiments, in which absorbance was measured in triplicate and averaged for each assay. The mean ± s.d. of the average absorbance in three independent knockdown experiments was plotted to draw the growth curves. Successful knock down of the ALK protein was confirmed by anti-ALK blots using α-tubulin blots as controls.

constructed in the pGCDNsamIRESKO retrovirus vector. Vector plasmids were co-transfected with vesicular stomatitis virus-G cDNA into 293GP cells to obtain a retrovirus-containing supernatant, which was then transduced into 293GPG cells to stable cell lines capable of producing vesicular stomatitis virus-G-pseudotyped retroviral particles on induction.

Functional analyses of a short-form ALK

To evaluate the phosphorylation status of the ALK mutants, stable clone cell lysates were subjected to western blot analysis with anti-ALK and the antibody-specific pTyr1604 (Cell Signaling Technology, Danvers, MA, USA) of ALK. Immunoprecipitation with antibodies to FLAG (Sigma, St Louis, MO, USA) were subjected to western blot analysis with a generic antiphosphotyrosine antibody (PY20). Western blot analyses were also performed using anti-ERK1/2, anti-phospho-ERK1/2, anti-AKT, anti-phospho-AKT, anti-STAT3 and anti-phospho-STAT3 antibodies (Cell Signaling Technology). AKT and STAT3 phosphorylation signals were quantitated by densitometric scanning using the ImageQuant 400 and ImageQuant TL software version 7 (GE Healthcare). The *in vitro* kinase assay was performed with the synthetic YFF peptide (Operon Biotechnologies, Reutlingen, Germany), as described previously,[36] using stable clones in pcDNA vector constructs. We also used the *in vitro* kinase assay for wild-type and mutant *ALK* expression in NIH3T3 cells by retrovirus-mediated gene transfer using the poly-GluTyr peptide. Cell extracts were immunoprecipitated with anti-Flag antibody, and the expression was subjected to immunoblotting using anti-ALK antibody. ALK mutant kinase activity was measured using a non-radioactive isotope solid-phase enzyme-linked immunosorbent assay in the Universal Tyrosine Kinase Assay kit (Takara Bio, Osaka, Japan). Assays were performed in 40 mM Tris (pH 7.4), 20 mM $MgCl_2$, 2 mM dithiothreitol and 0.1 mg/ml bovine serum albumin buffer.

Transforming potential of short-form ALK

For colony assays, 1×10^3 stably transfected NIH3T3 cells were mixed in 0.4% agarose with 10% fetal bovine serum–Dulbecco's modified Eagle's medium and plated on 0.6% agarose-coated 35-mm dishes. After culturing for 14 days, colonies measuring 0.1 mm in diameter were counted. Colonies were quantified during triplicate experiments. Tumor formation

Table 3. Primer sets used in this study

	Primer sequence (5′→3′)		*Annealing temperature (°C)*
	Forward	*Reverse*	
RT-PCR analyses			
ALK exon 1/5	CTTCTCTTCCAGATCTTCGG	ATTCAGGGCAAAGAAGTCCAC	55
Exon 1/2	AAGCAGTTGGTGCTGGAGCT	TTTGACTTCCCCTGTGAGCT	55
Exon 2/4	CATAGCTCCTTGGAATCACC	ATGAGGAGCAGCAGTGAGCA	55
Exon 4/5-6	TTCTCAACACCTCAGCTGAC	ACTGCAGTGAAGGAACATCC	55
Exon 5/8-9	GAAACCGCAGCTTGTCTGCA	CGATCAAGAGCTCTCCATGT	55
Exon 8/12	AAGTGCTACAGTGACCAGTG	TAGCGGAGAGGACAAGATC	55
Exon 11/14	ATATCTCCATCAGCCTGGAC	AAGAACACCATGATGCGGTC	55
Exon 13/15-16	CCTGAAAGGCATCCAGATCT	AAGATGAAGGATGGAGTGCC	55
Exon 15/17	AATCCGTGTGAACAGAAGCG	TGGAGGAGGCGGAGGATATA	55
Exon 17/19-20	AAATCTTTGCAGGAGGGTGC	GCGTCTCCTGCATTGTGTCA	55
Exon 20/23	TTTCTCCGGCATCATGATTG	CTCATGGAAGCCCTGATCAT	55
Exon 23/26	TGCCTGAAGTGTGCTCTGAA	GATTGGAGACTTCGGGATGG	55
Exon 26/30	AGAAACTGCCTCTTGACCTG	GGACCCGGATGTAATCAACA	55
Exon 29/30	GGAGAGGATTGAATACTGCA	GTTGCACAAGGTCCACGGAT	55
Exon 30/30	TGCAGAGATCTCTGTTCGAG	GTTGCACAAGGTCCACGGAT	55
Exon 30/30	TAACGTTGCAACTGGGAGAC	GTTGCACAAGGTCCACGGAT	55
β-Actin	CTTCTACAATGAGCTGCGTG	TCATGAGGTAGTCAGTCAGC	55
Southern blot analyses			
ALK exon 1	AGAGTCTGGCAGTTGACTTC	TGCTCACAAACAGTCCCGAAG	60
Exon 2	TCAACTCAGTCTACTGGTGG	GGATATGGCAGACACAAAGC	60
Exon 3	AGCCCTGTGGTATTGACAAC	AGATGGGACTTGTCTTCCTC	60
Exon 4	AGAATGGAGGAAGAAGGCTG	GTAATTGCTCAACCTGGACC	60
TUBA4A	CTCTCACACTCTGGTATCTC	CTGACCATTAGCACAGTCTC	60
Quantitative genomic PCR analyses			
ALK exon 1	CTCAGCGAGCTGTTCAGTTG	CAGTCCCGAAGATCTGGAAG	55
Intron 1	CTGCTTGGTTCCTCACATCC	GTCTGAGTCATTGGCTAATCTCA	55
Exon 2	ACCCAAGCACATGGATCAG	GATGAGACAGGAAAGGGAAGG	55
Intron 2	GGTATACACGTGCCATGGTG	CCAAATACGGCATGTTCTCA	55
Exon 3	GGAGTGCAGCTTTGACTTCC	CTGGGCATCTCCTTAGAACG	55
Intron 3	TGGCATGATTGATTACCCAAG	CTGGAGATCACCCTTTGAGG	55
Exon 4	CAACACCTCAGCTGACTCCA	CTCTCTTGCAGCCTCGTTG	55

Abbreviations: ALK, anaplastic lymphoma kinase; RT-PCR, reverse transcription-polymerase chain reaction.

assay was performed in nude mice, in which 1.0×10^7 NIH3T3 cells expressing wild-type *ALK* and *ALK*$^{del2-3}$ mutant were injected by the calcium phosphate method. Tumor formation was evaluated 21 days after inoculation as described previously.[6]

Immunofluorescence

Cells were fixed for 10 min with 4% paraformaldehyde and washed three times with phosphate-buffered saline. After 1 h of blocking in phosphate-buffered saline containing 4% donkey serum and 0.1% Triton X-100/phosphate-buffered saline, the cells were incubated for 2 h in the same buffer with polyclonal anti-ALK (Santa Cruz Biotechnology, Santa Cruz, CA, USA) and monoclonal anti-PDI (Abcam, Cambridge, MA, USA), respectively. The cells were then washed three times with phosphate-buffered saline before and after incubation with anti-mouse IgG Alexa Fluor 488 and anti-rabbit IgG Alexa Fluor 594-conjugated secondary antibodies, respectively, (Invitrogen, Carlsbad, CA, USA). The cells were then mounted in Prolong Gold (Invitrogen). Confocal laser microscopy was performed using a Fluoview 10 000 confocal microscope (Olympus, Tokyo, Japan). Colocalization of ALK and PDI was quantified using the Pearson's correlation coefficient and determined through correlation analysis with a Fluoview 1000 software.[37]

Deglycosylation of ALK with N-glycosidase F, N-glycosidase H and O-glycosidase

Proteins from cell lysates obtained from neuroblastoma cell lines NB-1 and NH-12 were incubated with N-glycosidase F and endoglycosidase H for deglycosylation (New England Biolabs, Ipswich, MA, USA), following the manufacturer's instructions.[18] The samples were then used for immunoblotting with anti-ALK antibody. Signal intensities of bands in the lane endoglycosidase H were quantified by densitometric scanning using the ImageQuant 400 and ImageQuant TL software version 7.

ALK inhibition by an ALK inhibitor and siRNA-mediated knockdown in neuroblastoma cells

A partial *ALK*-deleted neuroblastoma-derived cell line (NB-1), *ALK*-mutated neuroblastoma-derived cell lines (SK-N-SH and TGW) and a glioblastoma-derived cell line (H4) were cultured with varying concentrations of the ALK inhibitor TAE684,[8] and cell growth was measured using the CellTiter-Glo Luminescent Cell Viability Assay (Promega, Tokyo, Japan). NIH3T3 cells were used as a control. The IC_{50} value of TAE684 against NB-1 cells was calculated by nonlinear regression (variable slope) using the GraphPad Prism 5 software (GraphPad, La Jolla, CA, USA). NB-1 and NH-12 cells with wild-type ALK were transfected with either an *ALK*-specific siRNA or a nonspecific siRNA, as described previously.[7] To assess the effect of ALK knockdown on cell growth, cells were seeded in 96-well plates at a concentration of 1.0×10^4 cells per well 24 h before transfection and assayed using the Cell Counting kit-8 (Dojindo, Kumamoto, Japan). We also performed an siRNA-mediated ALK knockdown cell proliferation assay using a cell counter and 6-well plates. These cells were seeded in 6-well plates at a concentration of 2.0×10^5 cells per well 24 h before transfection. The number of cells was counted after 72 h using cytorecon (ECI, Tokyo, Japan).

Statistical analyses

The Mann-Whitney *U*-test was used to compare the differences in colony formation as well as the effects of ALK knockdown on cell growth between wild-type and ALK mutants. Phosphorylation signals of downstream molecules were evaluated by Student's *t*-test.

CONFLICT OF INTEREST

The authors declare no conflict of interest.

ACKNOWLEDGEMENTS

We thank Mrs Matsumura, Mrs Hoshino, Mrs Yin, Miss Ogino and Mrs Saito for their excellent technical assistance. We would also thank Dr Tanaka, Dr Saito, Mr Shiosaka and Mrs Mori for useful advice concerning biological analysis; Dr AT Look, Harvard Medical University, and Dr A Inoue, St Jude Children's Research Hospital, for their generous gifts of neuroblastoma cell lines. This work was supported by Research on Measures for Intractable Diseases, Health and Labor Sciences Research Grants, Ministry of Health, Labor and Welfare, Research on Health Sciences focusing on Drug Innovation, the Japan Health Sciences Foundation and Core Research for Evolutional Science and Technology, Japan Science and Technology Agency.

REFERENCES

1 Morris SW, Kirstein MN, Valentine MB, Dittmer K, Shapiro DN, Look AT *et al.* Fusion of a kinase gene, ALK, to a nucleolar protein gene, NPM, in non-Hodgkins-lymphoma (Vol 263, PG 1281, 1994). *Science* 1995; **267**: 316-317.
2 Shiota M, Nakamura S, Ichinohasama R, Abe M, Akagi T, Takeshita M *et al.* Anaplastic large-cell lymphomas expressing the novel chimeric protein P80(NPM/ALK)-a distinct clinicopathological entity. *Blood* 1995; **86**: 1954-1960.
3 Griffin CA, Hawkins AL, Dvorak C, Henkle C, Ellingham T, Perlman EJ. Recurrent involvement of 2p23 in inflammatory myofibroblastic tumors. *Cancer Res* 1999; **59**: 2776-2780.
4 Jazii FR, Najafi Z, Malekzadeh R, Conrads TP, Ziaee AA, Abnet C *et al.* Identification of squamous cell carcinoma associated proteins by proteomics and loss of beta tropomyosin expression in esophageal cancer. *World J Gastroenterol* 2006; **12**: 7104-7112.
5 Rikova K, Guo A, Zeng Q, Possemato A, Yu J, Haack H *et al.* Global survey of phosphotyrosine signaling identifies oncogenic kinases in lung cancer. *Cell* 2007; **131**: 1190-1203.
6 Soda M, Choi YL, Enomoto M, Takada S, Yamashita Y, Ishikawa S *et al.* Identification of the transforming EML4-ALK fusion gene in non-small-cell lung cancer. *Nature* 2007; **448**: 561-5U3.
7 Chen YY, Takita J, Choi YL, Kato M, Ohira M, Sanada M *et al.* Oncogenic mutations of ALK kinase in neuroblastoma. *Nature* 2008; **455**: 971-U56.
8 George RE, Sanda T, Hanna M, Frohling S, Luther W, Zhang JM *et al.* Activating mutations in ALK provide a therapeutic target in neuroblastoma. *Nature* 2008; **455**: 975-978.
9 Janoueix-Lerosey I, Lequin D, Brugieres L, Ribeiro A, de Pontual L, Combaret V *et al.* Somatic and germline activating mutations of the ALK kinase receptor in neuroblastoma. *Nature* 2008; **455**: 967-U51.
10 Mosse YP, Laudenslager M, Longo L, Cole KA, Wood A, Attiyeh EF *et al.* Identification of ALK as a major familial neuroblastoma predisposition gene. *Nature* 2008; **455**: 930-U22.
11 Maris JM, Hogarty MD, Bagatell R, Cohn SL. Neuroblastoma. *Lancet* 2007; **369**: 2106-2120.
12 De Bernardi B, Nicolas B, Boni L, Indolfi P, Carli M, di Montezemolo LC *et al.* Disseminated neuroblastoma in children older than one year at diagnosis: comparable results with three consecutive high-dose protocols adopted by the Italian Co-Operative Group for Neuroblastoma. *J Clin Oncol* 2003; **21**: 1592-1601.
13 Matthay KK, Villablanca JG, Seeger RC, Stram DO, Harris RE, Ramsay NK *et al.* Treatment of high-risk neuroblastoma with intensive chemotherapy, radiotherapy, autologous bone marrow transplantation, and 13-*cis*-retinoic acid. *N Engl J Med* 1999; **341**: 1165-1173.
14 Pearson ADJ, Pinkerton CR, Lewis IJ, Imeson J, Ellershaw C, Machin D *et al.* High-dose rapid and standard induction chemotherapy for patients aged over 1 year with stage 4 neuroblastoma: a randomised trial. *Lancet Oncol* 2008; **9**: 247-256.
15 Beckmann G, Bork P. An adhesive domain detected in functionally diverse receptors. *Trends Biochem Sci* 1993; **18**: 40-41.
16 Loren CE, Englund C, Grabbe C, Hallberg B, Hunter T, Palmer RH. A crucial role for the anaplastic lymphoma kinase receptor tyrosine kinase in gut development in *Drosophila melanogaster*. *EMBO Rep* 2003; **4**: 781-786.
17 Choudhary C, Olsen JV, Brandts C, Cox J, Reddy PNG, Boehmer FD *et al.* Mislocalized activation of oncogenic RTKs switches downstream signaling outcomes. *Mol Cell* 2009; **36**: 326-339.
18 Mazot P, Cazes A, Boutterin MC, Figueiredo A, Raynal V, Combaret V *et al.* The constitutive activity of the ALK mutated at positions F1174 or R1275 impairs receptor trafficking. *Oncogene* 2011; **30**: 2017-2025.
19 Lemmon MA, Schlessinger J. Cell signaling by receptor tyrosine kinases. *Cell* 2010; **141**: 1117-1134.
20 Lu Y, Yao HP, Wang MH. Multiple variants of the RON receptor tyrosine kinase: biochemical properties, tumorigenic activities, and potential drug targets. *Cancer Lett* 2007; **257**: 157-164.
21 Pedersen MW, Meltorn M, Damstrup L, Poulsen HS. The type III epidermal growth factor receptor mutation-biological significance and potential target for anti-cancer therapy. *Ann Oncol* 2001; **12**: 745-760.
22 Ekstrand AJ, James CD, Cavenee WK, Seliger B, Pettersson RF, Collins VP. Genes for epidermal growth-factor receptor, transforming growth factor-alpha, and epidermal growth-factor and their expression in human gliomas *in vivo*. *Cancer Res* 1991; **51**: 2164-2172.
23 Wong AJ, Ruppert JM, Bigner SH, Grzeschik CH, Humphrey PA, Bigner DS *et al.* Structural alterations of the epidermal growth-factor receptor gene in human gliomas. *Proc Natl Acad Sci USA* 1992; **89**: 2965-2969.
24 Gan HK, Kaye AH, Luwor RB. The EGFRvIII variant in glioblastoma multiforme. *J Clin Neurosci* 2009; **16**: 748-754.
25 Prigent SA, Nagane M, Lin H, Huvar I, Boss GR, Feramisco JR *et al.* Enhanced tumorigenic behavior of glioblastoma cells expressing a truncated epidermal growth factor receptor is mediated through the Ras-Shc-Grb2 pathway. *J Biol Chem* 1996; **271**: 25639-25645.
26 Zhou YQ, He C, Chen YQ, Wang D, Wang MH. Altered expression of the RON receptor tyrosine kinase in primary human colorectal adenocarcinomas: generation of different splicing RON variants and their oncogenic potential. *Oncogene* 2003; **22**: 186-197.
27 Ronsin C, Muscatelli F, Mattei MG, Breathnach R. A novel putative receptor protein tyrosine kinase of the met family. *Oncogene* 1993; **8**: 1195-1202.
28 Wang MH, Kurtz AL, Chen YQ. Identification of a novel splicing product of the RON receptor tyrosine kinase in human colorectal carcinoma cells. *Carcinogenesis* 2000; **21**: 1507-1512.
29 Chen YQ, Zhou YQ, Angeloni D, Kurtz AL, Qiang XZ, Wang MH. Overexpression and activation of the RON receptor tyrosine kinase in a panel of human colorectal carcinoma cell lines. *Exp Cell Res* 2000; **261**: 229-238.
30 Palmer RH, Vernersson E, Grabbe C, Hallberg B. Anaplastic lymphoma kinase: signalling in development and disease. *Biochem J* 2009; **420**: 345-361.
31 Chiarle R, Voena C, Ambrogio C, Piva R, Inghirami G. The anaplastic lymphoma kinase in the pathogenesis of cancer. *Nat Rev Cancer* 2008; **8**: 11-23.
32 Schulte JH, Bachmann HS, Brockmeyer B, DePreter K, Oberthur A, Ackermann S *et al.* High ALK receptor tyrosine kinase expression supersedes ALK mutation as a determining factor of an unfavorable phenotype in primary neuroblastoma. *Clin Cancer Res* 2011; **17**: 5082-5092.
33 Takita J, Yang HW, Chen YY, Hanada R, Yamamoto K, Teitz T *et al.* Allelic imbalance on chromosome 2q and alterations of the caspase 8 gene in neuroblastoma. *Oncogene* 2001; **20**: 4424-4432.
34 Brodeur GM, Pritchard J, Berthold F, Carlsen NLT, Castel V, Castleberry RP *et al.* Revisions of the international criteria for neuroblastoma diagnosis, staging, and response to treatment. *J Clin Oncol* 1993; **11**: 1466-1477.
35 Takita J, Hayashi Y, Nakajima T, Adachi J, Tanaka T, Yamaguchi N *et al.* The p16 (CDKN2A) gene is involved in the growth of neuroblastoma cells and its expression is associated with prognosis of neuroblastoma patients. *Oncogene* 1998; **17**: 3137-3143.
36 Donella-Deana A, Marin O, Cesaro L, Gunby RH, Ferrarese A, Coluccia AML *et al.* Unique substrate specificity of anaplastic lymphoma kinase (ALK): development of phosphoacceptor peptides for the assay of ALK activity. *Biochemistry* 2005; **44**: 8533-8542.
37 Smith JL, McBride CM, Nataraj PS, Bartos DC, January CT, Delisle BP. Trafficking-deficient hERG K(+) channels linked to long QT syndrome are regulated by a microtubule-dependent quality control compartment in the ER. *Am J Physiol-Cell Physiol* 2011; **301**: C75-C85.

Supplementary Information accompanies the paper on the Oncogene website (http://www.nature.com/onc)

Wnt3a stimulates maturation of impaired neutrophils developed from severe congenital neutropenia patient-derived pluripotent stem cells

Takafumi Hiramoto[a,b], Yasuhiro Ebihara[b,c,1], Yoko Mizoguchi[d], Kazuhiro Nakamura[d], Kiyoshi Yamaguchi[e], Kazuko Ueno[f], Naoki Nariai[f], Shinji Mochizuki[b,c], Shohei Yamamoto[b,c], Masao Nagasaki[f], Yoichi Furukawa[e], Kenzaburo Tani[a], Hiromitsu Nakauchi[g], Masao Kobayashi[d], and Kohichiro Tsuji[b,c]

[a]Division of Molecular and Clinical Genomics, Medical Institute of Bioregulation, Kyushu University, Higashi-ku, Fukuoka 812-8582, Japan; [c]Department of Pediatric Hematology/Oncology, Research Hospital, Divisions of [b]Stem Cell Processing and [g]Stem Cell Therapy, Center for Stem Cell Biology and Regenerative Medicine, and [e]Division of Clinical Genome Research, Advanced Clinical Research Center, Institute of Medical Science, University of Tokyo, Minato-ku, Tokyo 108-8639, Japan; [d]Pediatrics, Hiroshima University Graduate School of Biomedical and Health Sciences, Minami-ku, Hiroshima 734-8551, Japan; and [f]Department of Integrative Genomics, Tohoku Medical Megabank Organization, Tohoku University, Aramaki, Aoba-ku, Sendai 980-8573, Japan

Edited by George Q. Daley, Children's Hospital Boston, Boston, MA, and accepted by the Editorial Board January 4, 2013 (received for review October 1, 2012)

The derivation of induced pluripotent stem (iPS) cells from individuals of genetic disorders offers new opportunities for basic research into these diseases and the development of therapeutic compounds. Severe congenital neutropenia (SCN) is a serious disorder characterized by severe neutropenia at birth. SCN is associated with heterozygous mutations in the neutrophil elastase [elastase, neutrophil-expressed (ELANE)] gene, but the mechanisms that disrupt neutrophil development have not yet been clarified because of the current lack of an appropriate disease model. Here, we generated iPS cells from an individual with SCN (SCN-iPS cells). Granulopoiesis from SCN-iPS cells revealed neutrophil maturation arrest and little sensitivity to granulocyte-colony stimulating factor, reflecting a disease status of SCN. Molecular analysis of the granulopoiesis from the SCN-iPS cells vs. control iPS cells showed reduced expression of genes related to the wingless-type mmtv integration site family, member 3a (Wnt3a)/β-catenin pathway [e.g., lymphoid enhancer-binding factor 1], whereas Wnt3a administration induced elevation lymphoid enhancer-binding factor 1-expression and the maturation of SCN-iPS cell-derived neutrophils. These results indicate that SCN-iPS cells provide a useful disease model for SCN, and the activation of the Wnt3a/β-catenin pathway may offer a novel therapy for SCN with ELANE mutation.

apoptosis | unfolded protein response | SCN disease model

Severe congenital neutropenia (SCN) is a heterogeneous bone marrow (BM) failure syndrome characterized by severe neutropenia at birth, leading to recurrent infections by bacteria or fungi (1). SCN patients reveal an arrest in neutrophil differentiation in the BM at the promyelocyte or myelocyte stage (1), as well as a propensity to develop myelodysplastic syndrome and acute myeloid leukemia (2). Current treatment by high-dose granulocyte-colony stimulating factor (G-CSF) administration induces an increase in the number of mature neutrophils in the peripheral blood of most SCN patients (3). Although this treatment is curative for the severe infections, there is a concern that high-dose G-CSF may increase the risk of hematologic malignancy in these individuals (4).

Several genetic mutations have been identified in SCN patients. Approximately 50% of autosomal-dominant SCN cases were shown to have various heterozygous mutations in the gene encoding neutrophil elastase [elastase, neutrophil-expressed (ELANE)] (5, 6), a monomeric, 218-amino acid (25 kDa) chymotryptic serine protease (7) that is synthesized during the early stages of primary granule production in promyelocytes (8, 9). However, the mechanism(s) causing impaired neutrophil maturation in SCN patients remains unclear due to the current lack of an appropriate disease model.

Results and Discussion

In the present study, we generated induced pluripotent stem (iPS) cells from the BM cells obtained from an SCN patient with a heterologous ELANE gene mutation (exon 5, 707 region, C194X) (SCN-iPS cells) to provide the basis for an SCN disease model. The patient who donated BM cells recurrently suffered from severe infections without exogenous G-CSF administration, but the G-CSF administration once a week prevented his repeated infection. The SCN-iPS cells continued to show embryonic stem cell morphology after >20 passages and also expressed pluripotent markers (Fig. S1*A*). The silencing of exogenous genes and the capability to differentiate into three germ layers by teratoma formation were confirmed for each of the three SCN-iPS cell clones (Fig. S1 *B* and *C*). Furthermore, the same ELANE gene mutation that was present in the patient persisted in the SCN-iPS cells (Fig. S1*D*). The SCN-iPS cells, as well as control iPS cells that were generated from healthy donors, had the normal karyotype (Fig. S1*E*) (10, 11) and no mutations in the mutation-sensitive region of the G-CSF receptor gene (12).

We first compared the hematopoietic differentiation from SCN-iPS cells with that from control iPS cells that were generated from healthy donors. SCN-iPS and control iPS cells were cocultured with a 15-Gy-irradiated murine stromal cell line (the AGM-S3 cell line), as reported (13). After 12 d, the cocultured cells were harvested, and the $CD34^+$ cells separated from these cells (SCN-iPS–$CD34^+$ and control iPS–$CD34^+$ cells, respectively) were cultured in a hematopoietic colony assay by using a cytokine mixture (*Materials and Methods*). The number and size of the erythroid (E) and mixed-lineage (Mix) colonies derived from SCN-iPS–$CD34^+$ cells (1×10^4 cells) were nearly identical to those of the corresponding colonies derived from control iPS–$CD34^+$ cells (E colonies: SCN-iPS cells, 11.0 ± 3.0, and control iPS cells, 11.4 ± 3.9; Mix colonies: SCN-iPS cells, 25.1 ± 7.2, and control iPS cells, 17.4 ± 4.0) (Fig. 1 *B* and *C* and Fig. S2 *A* and *B*). However, the number of myeloid colonies derived from SCN-iPS–$CD34^+$ vs. control iPS–$CD34^+$ cells was significantly lower (SCN-iPS cells, 47.4 ± 19.5; control iPS cells, 127.8 ± 17.9; $P < 0.01$), and the size of the colonies was also smaller (Fig. 1 *A*

Author contributions: T.H., Y.E., K.Y., S.M., S.Y., Y.F., K. Tani, H.N., M.K., and K. Tsuji designed research; T.H., Y.M., K.N., and K.Y. performed research; T.H., Y.E., Y.M., K.N., K.Y., K.U., N.N., S.M., S.Y., M.N., and K. Tsuji analyzed data; and T.H., Y.E., and K. Tsuji wrote the paper.

The authors declare no conflict of interest.

This article is a PNAS Direct Submission. G.Q.D. is a guest editor invited by the Editorial Board.

[1]To whom correspondence should be addressed. E-mail: ebihara@ims.u-tokyo.ac.jp.

This article contains supporting information online at www.pnas.org/lookup/suppl/doi:10.1073/pnas.1217039110/-/DCSupplemental.

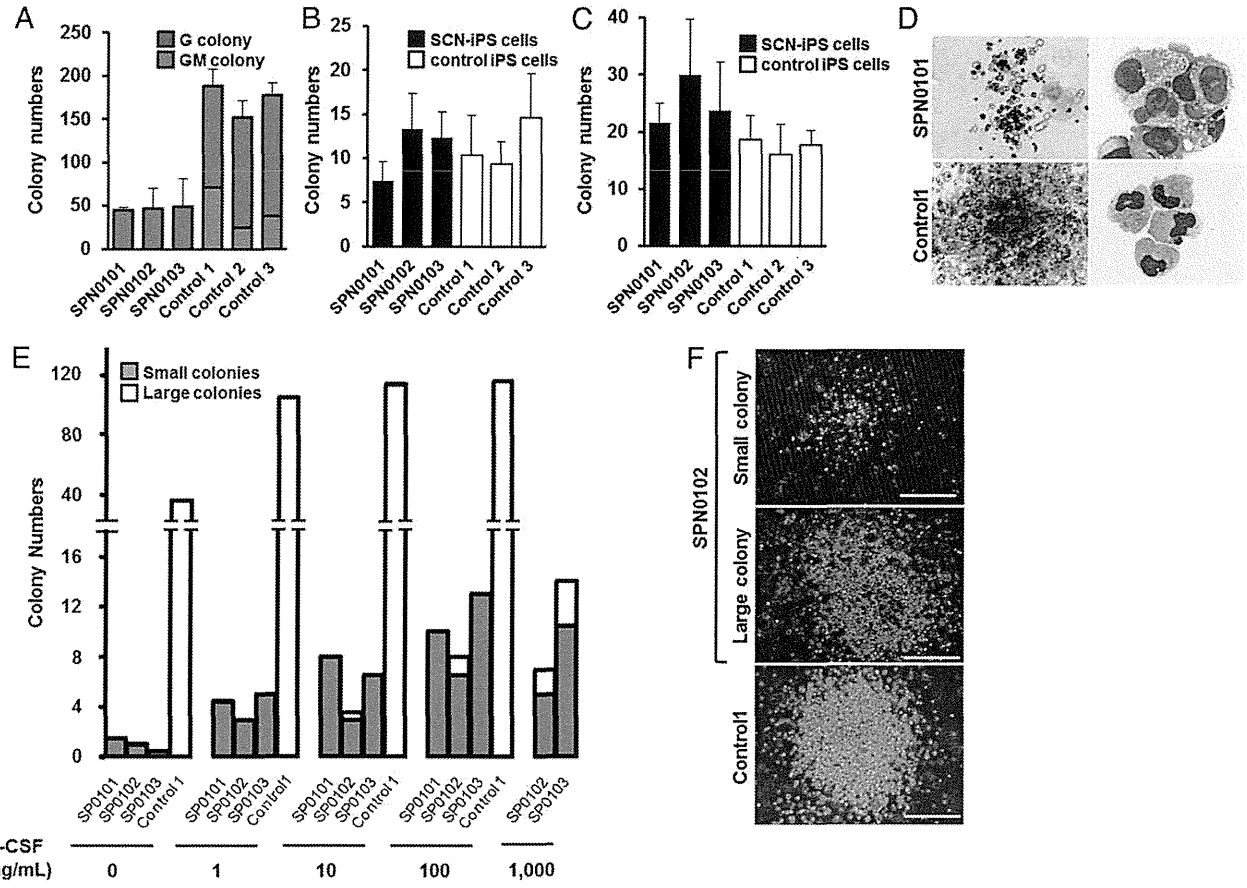

Fig. 1. Impaired neutrophil development from SCN-iPS cells. (*A*–*C*) A hematopoietic colony assay was performed by using 1×10^4 $CD34^+$ cells derived from three SCN-iPS cell clones (SPN0101, SPN0102, and SPN0103) and three control iPS cell clones (controls 1, 2, and 3) in the presence of a cytokine mixture. Colonies were sorted as myeloid (*A*), erythroid (*B*), and mixed-lineage (Mix) (*C*). Data are shown as mean ± SD. (*D*) Photographs of colonies (*Left*; 100×) and cells in a GM colony (*Right*; 400×; May–Grünwald–Giemsa staining). (*E*) A hematopoietic colony assay with dose escalation of G-CSF was performed by using 1×10^5 $CD34^+$ cells derived from SCN-iPS and control iPS cells. Filled and open bars indicate small colonies consisting of <100 cells and large colonies consisting of >100 cells, respectively. Data are shown as the average of three independent experiments. (*F*) Photographs of a small colony derived from SCN-iPS cells (SPN0102) in the presence of 10 ng/mL G-CSF, large colonies derived from SCN-iPS cells in the presence of 1,000 ng/mL G-CSF, and large colonies derived from control iPS cells (control 1) in the presence of 10 ng/mL G-CSF. (Scale bars, 200 μm.)

and *D*). In particular, only a few SCN-iPS cell-derived granulocyte (G) colonies—myeloid colonies consisting of only granulocytes—were detected (Fig. 1*A*). SCN-iPS cell-derived granulocyte–macrophage (GM) colonies—myeloid colonies consisting of macrophages/monocytes with/without granulocytes—contained a few immature myeloid cells in addition to macrophages/monocytes, whereas control iPS cell-derived GM colonies included a substantial number of mature, segmented, and band neutrophils (Fig. 1*D*).

We also found that Mix colonies derived from SCN-iPS cells, but not control iPS cells, contained immature myeloid cells and few mature neutrophils (Fig. S2 *C* and *D*). Next, we conducted a hematopoietic colony assay using various concentrations of G-CSF alone instead of the cytokine mixture to examine the G-CSF dose dependency of neutrophil differentiation from SCN-iPS and control iPS–$CD34^+$ cells. For all concentrations of G-CSF used (1–1,000 ng/mL), the SCN-iPS cell-derived myeloid colonies were significantly lower in number and smaller in size than the control iPS cell-derived myeloid colonies (Fig. 1*E*). Myeloid colony formation from control iPS cells reached a plateau at ~1–10 ng/mL G-CSF, whereas the number and size of those from SCN-iPS cells gradually increased with increasing concentrations of G-CSF. However, the values observed for SCN-iPS cells did not reach those for the control iPS cells, even at the highest dose of G-CSF used (1,000 ng/mL). Furthermore, large colonies consisting of >100 cells derived from SCN-iPS cells were only found with higher concentrations of G-CSF (Fig. 1*F*). Thus, granulopoiesis initiated from SCN-iPS cells was relatively insensitive to G-CSF, reflecting the inadequate in vivo response of neutrophils to G-CSF in SCN patients (14, 15). Therefore, these results support the applicability of the SCN-iPS cells established herein as a disease model for SCN.

To examine neutrophil development from SCN-iPS cells in more detail, SCN-iPS and control iPS–$CD34^+$ cells (1×10^4 cells each) were cocultured in suspension with AGM-S3 cells in the presence of neutrophil differentiation medium (*SI Materials and Methods*). The number of nonadherent cells derived from SCN-iPS–$CD34^+$ cells was lower than that from control iPS–$CD34^+$ cells on day 14 of culture (SCN-iPS cells, $9.77 \times 10^4 \pm 1.65 \times 10^4$ cells; control iPS cells, $52.48 \times 10^4 \pm 23.13 \times 10^4$ cells; $P < 0.05$) (Fig. 2*A*). The proportion of mature neutrophils among the nonadherent cells was also significantly lower for SCN-iPS cells relative to control iPS cells on day 14 (SPN-iPS cells, 15.53% ± 4.33%; control iPS cells, 71.285 ± 3.30%; $P < 0.05$) (Fig. 2 *B* and *C*), indicating that myeloid cells derived from SCN-iPS cells revealed the maturation arrest in the neutrophil development. We then examined a possibility that the maturation arrest in SCN-

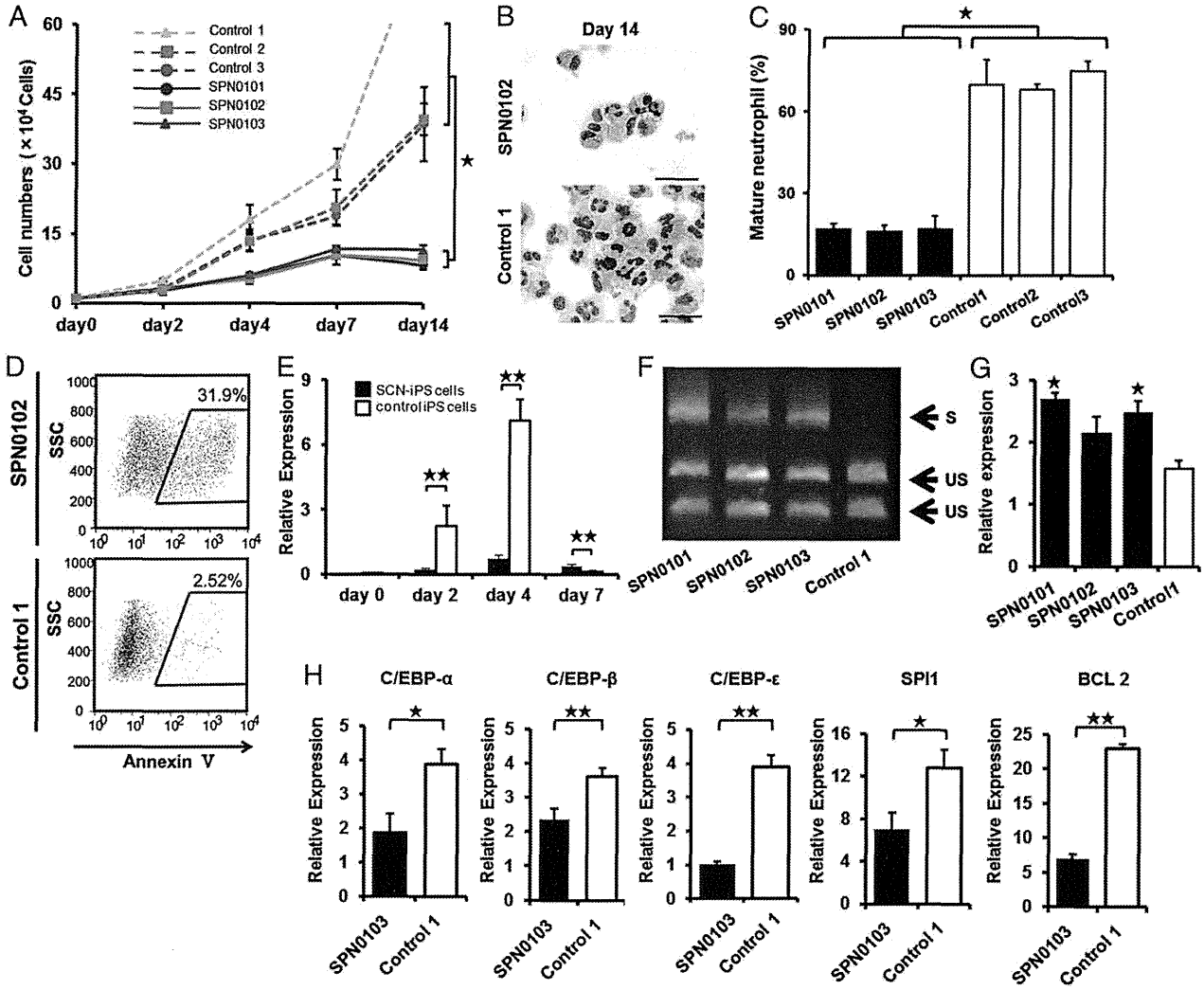

Fig. 2. Analysis of impaired neutrophil development from SCN-iPS cells. (*A*) Total number of nonadherent cells in the suspension culture of 1×10^4 $CD34^+$ cells derived from SCN-iPS and control iPS cells. Data are shown as mean ± SD. $^*P < 0.01$. (*B*) Photographs of nonadherent cells derived from SCN-iPS (SPN0103) and control iPS cells (control 1) on day 14 of culture (400×; May–Grünwald–Giemsa staining; scale bars, 50 μm.) (*C*) Filled and open bars show the proportion of mature neutrophils among the cells derived from SCN-iPS (filled bars) and control iPS (open bars) cells on day 14 of suspension culture. Data are shown as mean ± SD. $^*P < 0.05$. (*D*) Flow cytometric analysis of annexin V expression on cultured cells from SCN-iPS cells (SPN0102) or control iPS cells (control 1) on day 7. (*E*) Sequential qRT-PCR analysis of the relative expression of ELANE mRNA [ELANE/hypoxanthine–guanine phosphoribosyltransferase (HPRT) expression]. Data obtained from independent experiments using three SCN-iPS cell clones (SPN0101, SPN0102, and SPN0103) and three control iPS cell clones are shown as mean ± SD. $^{**}P < 0.01$. (*F* and *G*) $CD34^+$ cells derived from SCN-iPS or control iPS cells were cultured in neutrophil differentiation medium (see text). On day 7, nonadherent cells were collected and analyzed. (*F*) Representative gel showing spliced (S) and unspliced (US) XBP-1 bands on day 7. (*G*) qRT-PCR analysis of the relative mRNA expression (target/HPRT expression) of BiP on day 7. Data are shown as mean ± SD. $^*P < 0.05$; different from control 1). (*H*) qRT-PCR analysis of the relative mRNA expression (target / HPRT expression) of C/EBP-α, C/EBP-β, C/EBP-ε, SPI1, and BCL2 genes in non-adherent cells derived from SCN-iPS cells (filled bars, SPN0103) and control iPS cells (open bars, control 1) on day 2 of suspension culture. Data are shown as the mean ± the s.d. ($^{**}P < 0.01$, $^*P < 0.05$).

iPS cell-derived myeloid cells might be caused by their apoptosis. In flow cytometric analysis, SCN-iPS cell-derived myeloid cells contained a significantly higher proportion of annexin V-positive cells than control iPS-derived myeloid cells on day 7 of culture, suggesting that the maturation arrest in myeloid cells derived from SCN-iPS cells might be caused by their apoptosis (Fig. 2*D*).

We next examined ELANE mRNA expression levels in nonadherent cells derived from SCN-iPS vs. control iPS cells (Fig. 2*E*). ELANE expression was significantly lower in nonadherent cells derived from SCN-iPS vs. control iPS cells on days 2 and 4 of culture ($P < 0.01$), as reported (16, 17). However, the former was a little higher than the latter on day 7 ($P < 0.01$). This result may be explained by the existence of SCN-iPS cell-derived myeloid cells arrested at an early stage along the neutrophil differentiation pathway even on day 7 of culture. We also examined the expression of proteinase 3 and azurocidin, which comprise a family of closely related genes encoding neutrophil granule proteins along with ELANE, and found these genes were more highly expressed on day 4 (Fig. S3).

It has been reported that induction of the endoplasmic reticulum stress (ER) response and the unfolded protein response (UPR) has been advanced as a potential explanation for the molecular pathogenesis of SCN (18, 19). Thus, we examined activation of the UPR by X-box binding protein 1 (XBP-1) mRNA splicing on day 7. As shown in Fig. 2*F*, SPN-iPS cells induced XBP-1 mRNA splicing. We also found the up-regulation of BiP

(also known as GRP78 or HSPA5) (Fig. 2*G*). These results suggested that ER stress response and UPR might be involved in the pathogenesis in SCN.

To examine further the differences in gene expression between the two cell types, a microarray analysis was carried out by using $CD34^+$ cells derived from SCN-iPS and control iPS cells (three clones of each) in suspension culture on day 2. At this early time point, differences in cell number and morphology were not yet readily discernible between SCN-iPS and control iPS cells, as shown in Fig. 2*A*. However, the microarray analysis revealed a differential expression of various genes between the two cell types. Transcription factor genes, which were related to neutrophil development [e.g., CCAAT/enhancer-binding protein (C/EBP)-α (20), C/EBP-β (21), C/EBP-ε (22), and SPI1 (also known as PU.1) (23)], were all down-regulated in SCN-iPS cells. B-cell chronic lymphocytic leukemia/lymphoma 2, which regulates cell death under ER stress through the core mitochondrial apoptosis pathway (24), was also down-regulated (Fig. 3*A*). These findings were confirmed by quantitative reverse-transcriptional PCR (qRT-PCR), as shown in Fig. 2*H*.

Notably, the down-regulation of the genes in SCN-iPS cells related to and regulated by the wingless-type mmtv integration site family, member 3a (Wnt3a)/β-catenin pathway [e.g., Wnt3a, lymphoid enhance-binding factor (LEF)-1, BIRC5 (also known as survivin), and cyclin D1] was also uncovered by microarray analysis and qRT-PCR (Fig. 3 *A*–*C* and Fig. S4). Therefore, we examined the effect of enhancement of Wnt3a/β-catenin signaling by exogenous Wnt3a addition on the neutrophil development of $CD34^+$ cells derived from SCN-iPS and control iPS cells. Although Wnt3a did not stimulate the survival, proliferation, and differentiation of $CD34^+$ cells derived from both iPS cells in the absence of cytokines stimulating myelopoiesis including G-CSF, the addition of Wnt3a to the neutrophil differentiation medium induced a dose-dependent increase in the percentage of mature neutrophils among the cultured cells, as shown in Fig. 3 *D* and *E*. Furthermore, when Wnt3a was added concurrently with 1,000ng/mL G-CSF, the proportion of mature neutrophils increased more than it did with Wnt3a or 1,000 ng/mL G-CSF alone, reaching a value comparable with that observed for control iPS cells (Fig. 4 *A* and *B*).

The reduced expression of LEF-1 (as regulated by the Wnt3a/β-catenin pathway) reportedly plays a critical role in the defective maturation of neutrophils in SCN patients (25). Therefore, we next examined LEF-1 mRNA expression in SCN-iPS–$CD34^+$ cells cultured in the presence of Wnt3a, G-CSF (1,000 ng/mL), or both. Wnt3a and G-CSF both enhanced LEF-1 mRNA expression, but the most significant increase was observed in the presence of Wnt3a plus G-CSF. LEF-1 expression in SCN-iPS–$CD34^+$ cells in response to Wnt3a plus G-CSF was almost the same as that in control iPS–$CD34^+$ cells (Fig. 4*C*). These results substantiate the importance of LEF-1 in neutrophil development and the pathogenesis of SCN, as shown (25). Moreover the

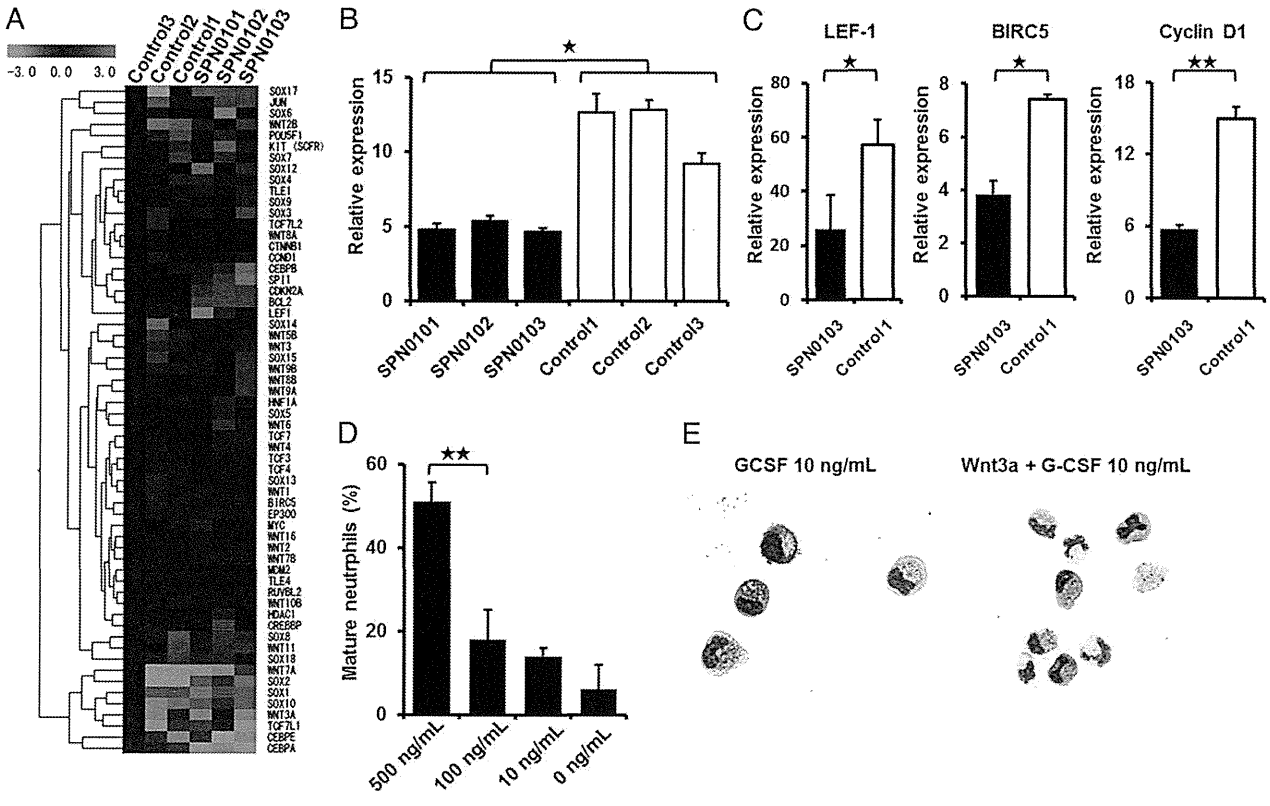

Fig. 3. Effects of Wnt3a on neutrophil development from SCN-iPS cells. (*A*) Heat map showing differential gene expression among SCN-iPS and control iPS cells on day 2. Red, high gene expression; blue, low gene expression compared with gene expression in control 3. (*B*) qRT-PCR analysis of the relative mRNA expression (target/HPRT expression) of Wnt3a on day 2. Filled and open bars indicate experiments using SCN-iPS cells (SPN0101, SPN0102, and SPN0103) and control iPS cells (controls 1, 2, and 3), respectively. Data are shown as mean ± SD. $^*P < 0.05$. (*C*) qRT-PCR analysis of the relative expression (target/HPRT expression) of genes regulated by the Wnt3a/β-catenin pathway (LEF-1, survivin, and cyclin D1) in SCN-iPS cells (filled bars, SPN0103) vs. control iPS cells (open bars, control 1) on day 2 of suspension culture. Data are shown as mean ± SD. $^{**}P < 0.01$; $^*P < 0.05$. (*D*) Proportion of mature neutrophils among the cells derived from SCN-iPS cells (SPN0102) on day 14 of suspension culture with dose escalation of Wnt3a. Data are shown as mean ± SD. $^{**}P < 0.01$. (*E*) Photographs of nonadherent cells on day 7 of suspension culture with or without Wnt3a (500 ng/mL) (400×; May–Grünwald–Giemsa staining).

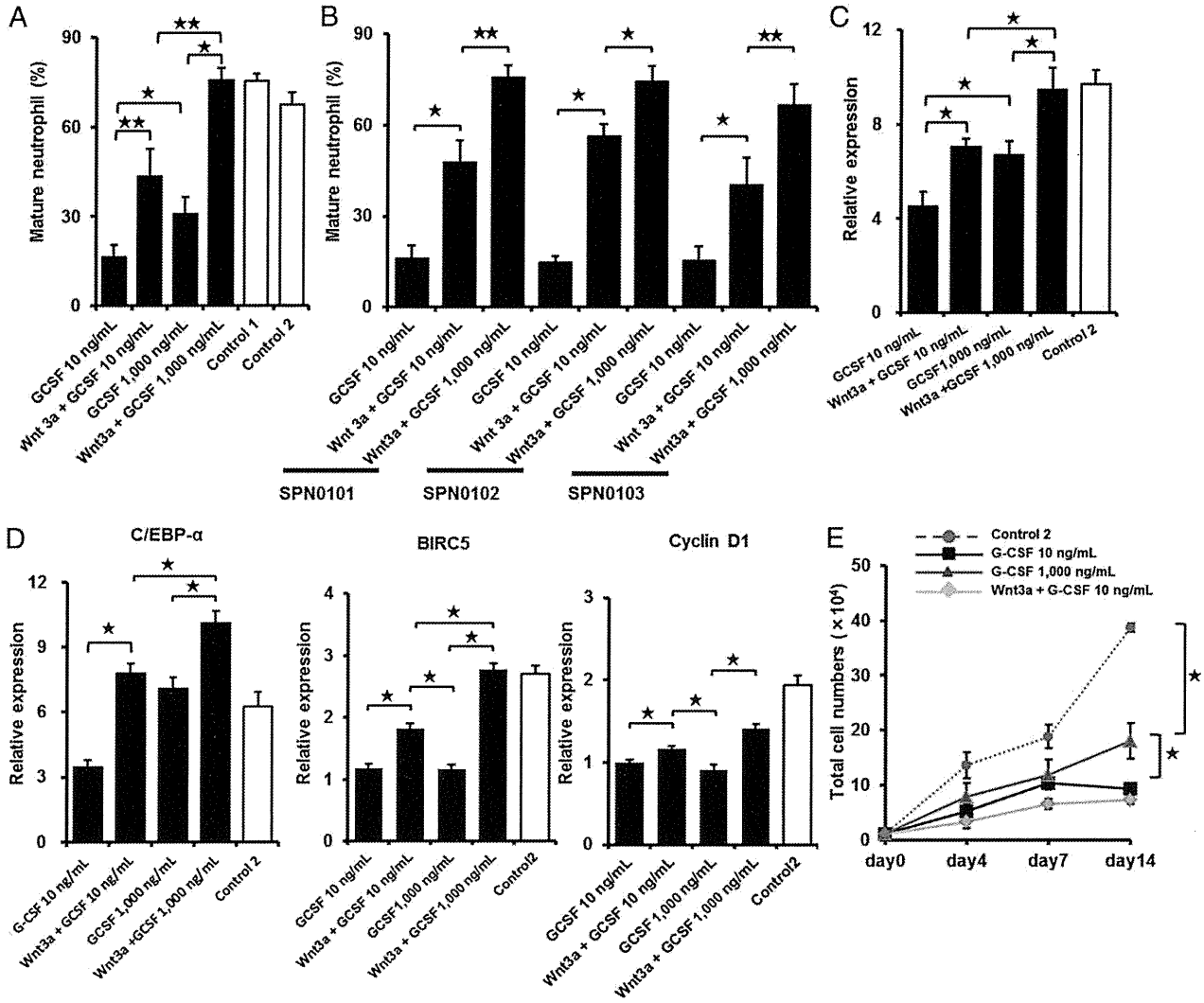

Fig. 4. Effects of Wnt3a in combination with high-dose G-CSF. (*A*) Filled and open bars show the proportion of mature neutrophils among the cells derived from SCN-iPS cells (SPN0101) on day 14 of suspension culture in the presence of neutrophil differentiation medium containing 10 ng/mL G-CSF (GCSF 10 ng/mL); 500 ng/mL Wnt3a and 10 ng/mL G-CSF (Wnt3a+GCSF 10 ng/mL); 1,000 ng/mL G-CSF (GCSF 1,000 ng/mL); or 500 ng/mL Wnt3a and 1,000 ng/mL G-CSF (Wnt3a + GCSF 1,000 ng/mL); and that from control iPS cells (controls 1 and 2) cultured in the neutrophil differentiation medium containing 10 ng/mL G-CSF, respectively. Data are shown as mean ± SD. $^{**}P < 0.01$; $^{*}P < 0.05$. (*B*) The proportion of mature neutrophils among the cells derived from three SCN-iPS cell clones (SPN0101, SPN0102, and SPN0103) on day 14 of suspension culture in the presence of neutrophil differentiation medium containing 10 ng/mL G-CSF (GCSF 10 ng/mL); 500 ng/mL Wnt3a and 10 ng/mL G-CSF (Wnt3a+GCSF 10 ng/mL); or 500 ng/mL Wnt3a and 1,000 ng/mL G-CSF (Wnt3a + GCSF 1,000 ng/mL). Data are shown as mean ± SD. $^{**}P < 0.01$; $^{*}P < 0.05$. (*C*) Filled and open bars show the relative expression (target/HPRT expression) of LEF-1 mRNA in SCN-iPS cells (SPN0101) on day 2 of suspension culture in the presence of differentiation medium containing the same combinations of Wnt3a and G-CSF as shown in *A* and that from control iPS cells (control 2), respectively. Data are shown as mean ± SD. $^{**}P < 0.01$; $^{*}P < 0.05$. (*D*) Filled and open bars show the relative expression (target/HPRT expression) of C/EBP-α, BIRC5, or cyclin D1 mRNA in SCN-iPS cells (SPN0101) on day 2 of suspension culture in the presence of differentiation medium containing the same combinations of Wnt3a and G-CSF as shown in *A* and that from control iPS cells (control 2), respectively. Data are shown as mean ± SD. $^{**}P < 0.01$; $^{*}P < 0.05$. (*E*) Total cell numbers of nonadherent cells in suspension cultures of 1×10^4 $CD34^+$ cells derived from control iPS cells (control 2; red broken line) and SCN-iPS cells (SPN0101) in the presence of neutrophil differentiation medium (black line) and those from SCN-iPS cells in the presence of neutrophil differentiation medium containing 500 ng/mL Wnt3a (yellow line) or 1,000 ng/mL G-CSF (black line). Data are shown as mean ± SD. $^{**}P < 0.05$.

administration of Wnt3a led to up-regulate C/EBP-α, cyclin D1, and BIRC5/survivin in addition to LEF-1 in the presence of G-CSF (Fig. 4*D*). These results suggested that the up-regulation of LEF-1 expression might promote granulopoiesis by increasing the expressions of cyclin D1, BIRC5/survivin, and C/EBP-α and its binding to LEF-1 in accordance with the previous report (25). Interestingly, Wnt3a did not stimulate the proliferation of myeloid cells, whereas 1,000 ng/mL G-CSF did to a certain extent (Fig. 4*E*). Hence, Wnt3a was capable of stimulating the maturation of impaired neutrophils in the presence of G-CSF, but not the proliferation of myeloid cells from SCN-iPS cells.

Importantly, aside from providing new insights into the mechanisms behind impaired neutrophil development in SCN patients, the present study demonstrates that agents activating the Wnt3a/β-catenin pathway are potential candidates for new drugs for SCN with mutations in the ELANE gene. Because endogenous G-CSF is readily increased in SCN patients (26), these activating agents may be viable alternatives to exogenous G-CSF treatment.

Materials and Methods

Additional information is available in *SI Materials and Methods*.

Generation of Human iPS Cells. BM fibroblasts from a patient with SCN and skin dermal fibroblasts from a healthy donor were acquired after obtaining informed consent after getting the approval by the Ethics Committee of the Institute of Medical Science, University of Tokyo, in accordance with the Declaration of Helsinki. The SCN patient presented with a heterozygous mutation in the ELANE gene in the 707 region of exon 5. SCN-iPS cells were established from the SCN-BM fibroblasts by transfection with the pMX retroviral vector, as described (10). This vector expressed the human transcription factors OCT3/4, SOX2, KLF4, and c-MYC. Control iPS cell clones, control 1 (TkDN4-M) and control 3 (201B7), were gifts from K. Eto and S. Yamanaka (Kyoto University, Kyoto), respectively (10, 11). Control 2 (SPH0101) was newly generated from another healthy donor's skin dermal fibroblasts by using the same methods.

Hematopoietic Colony Assay. A hematopoietic colony assay was performed in an aliquot of culture mixture, which contained 1.2% methylcellulose (Shin-Etsu Chemical), 30% (vol/vol) FBS, 1% (vol/vol) deionized fraction V BSA, 0.1 mM 2-mercaptoethanol (2-ME), α-minimum essential medium, and a cytokine mixture consisting of 100 ng/mL human stem cell factor (hSCF) (Wako), 100 ng/mL fusion protein 6 [FP6; a fusion protein of interleukin (IL)-6 and IL-6 receptor] (a gift from Tosoh), 10 ng/mL human IL-3 (hIL-3) (a gift from Kirin Brewery), 10 ng/mL human thrombopoietin (hTPO) (a gift from Kirin Brewery), 10 ng/mL human G-CSF (a gift from Chugai Pharmaceutical), and 5 U/mL human erythropoietin (a gift from Kirin Brewery). For dose escalation experiments, various concentrations (0, 1, 10, 100, and 1,000 ng/mL) of G-CSF were used instead of the cytokine mixture described above. Colony types were determined according to established criteria on day 14 of culture by in situ observations under an inverted microscope (IX70; Olympus) (27).

Suspension Culture and Neutrophil Differentiation Assay. $CD34^+$ cells (1×10^4 cells) were cocultured with irradiate confluent AGM-S3 cells in neutrophil differentiation medium containing Iscove's modified Dulbecco's medium, 10% FBS, 3 mM L-glutamine, 1×10^{-4} M 2-ME, 1×10^{-4} M nonessential amino acids solution, 100 ng/mL hSCF, 100 ng/mL FP6, 10 ng/mL hIL-3, 10 ng/mL hTPO, and 10 or 1,000 ng/mL human G-CSF. Wnt3a (10, 100, or 500 ng/mL) (R&D) was then added. The medium was replaced with an equivalent volume of fresh medium every 4 d. Living, nonadherent cells were counted following 0.4% trypan blue staining.

PCR primer. All primer sets used in this study are shown in Table S1.

Statistical Analysis. All data are presented as mean ± SD. $P < 0.05$ was considered significant. Statistical analyses were performed by using Prism software (GraphPad).

ACKNOWLEDGMENTS. We thank the individual with SCN who participated in this study; K. Eto for providing control iPS cells (control 1; TkDN4-M); S. Yamanaka for providing control iPS cells (control 3; 206B7); and E. Matsuzaka and S. Hanada for technical assistance. This work was supported by in part by Ministry of Education, Culture, Sports, Science, and Technology of Japan (MEXT) Grants-in-Aid (to Y.E.) and Project for Realization of Regenerative Medicine (MEXT) Grants-in-Aid (to K.Tsuji).

1. Zeidler C, Germeshausen M, Klein C, Welte K (2009) Clinical implications of *ELA2-*, *HAX1-*, and G-CSF-receptor (*CSF3R*) mutations in severe congenital neutropenia. *Br J Haematol* 144(4):459–467.
2. Freedman MH, et al. (2000) Myelodysplasia syndrome and acute myeloid leukemia in patients with congenital neutropenia receiving G-CSF therapy. *Blood* 96(2):429–436.
3. Dale DC, et al. (1993) A randomized controlled phase III trial of recombinant human granulocyte colony-stimulating factor (filgrastim) for treatment of severe chronic neutropenia. *Blood* 81(10):2496–2502.
4. Rosenberg PS, et al.; Severe Chronic Neutropenia International Registry (2006) The incidence of leukemia and mortality from sepsis in patients with severe congenital neutropenia receiving long-term G-CSF therapy. *Blood* 107(12):4628–4635.
5. Xia J, et al. (2009) Prevalence of mutations in ELANE, GFI1, HAX1, SBDS, WAS and G6PC3 in patients with severe congenital neutropenia. *Br J Haematol* 147(4):535–542.
6. Horwitz MS, et al. (2007) Neutrophil elastase in cyclic and severe congenital neutropenia. *Blood* 109(5):1817–1824.
7. Hajjar E, Broemstrup T, Kantari C, Witko-Sarsat V, Reuter N (2010) Structures of human proteinase 3 and neutrophil elastase—so similar yet so different. *FEBS J* 277(10): 2238–2254.
8. Fouret P, et al. (1989) Expression of the neutrophil elastase gene during human bone marrow cell differentiation. *J Exp Med* 169(3):833–845.
9. Pham CT (2006) Neutrophil serine proteases: Specific regulators of inflammation. *Nat Rev Immunol* 6(7):541–550.
10. Takayama N, et al. (2010) Transient activation of c-MYC expression is critical for efficient platelet generation from human induced pluripotent stem cells. *J Exp Med* 207(13):2817–2830.
11. Takahashi K, et al. (2007) Induction of pluripotent stem cells from adult human fibroblasts by defined factors. *Cell* 131(5):861–872.
12. Germeshausen M, Ballmaier M, Welte K (2007) Incidence of CSF3R mutations in severe congenital neutropenia and relevance for leukemogenesis: Results of a long-term survey. *Blood* 109(1):93–99.
13. Ma F, et al. (2007) Novel method for efficient production of multipotential hematopoietic progenitors from human embryonic stem cells. *Int J Hematol* 85(5):371–379.
14. Konishi N, et al. (1999) Defective proliferation of primitive myeloid progenitor cells in patients with severe congenital neutropenia. *Blood* 94(12):4077–4083.
15. Nakamura K, et al. (2000) Abnormalities of primitive myeloid progenitor cells expressing granulocyte colony-stimulating factor receptor in patients with severe congenital neutropenia. *Blood* 96(13):4366–4369.
16. Skokowa J, Fobiwe JP, Dan L, Thakur BK, Welte K (2009) Neutrophil elastase is severely down-regulated in severe congenital neutropenia independent of ELA2 or HAX1 mutations but dependent on LEF-1. *Blood* 114(14):3044–3051.
17. Kawaguchi H, et al. (2003) Dysregulation of transcriptions in primary granule constituents during myeloid proliferation and differentiation in patients with severe congenital neutropenia. *J Leukoc Biol* 73(2):225–234.
18. Köllner I, et al. (2006) Mutations in neutrophil elastase causing congenital neutropenia lead to cytoplasmic protein accumulation and induction of the unfolded protein response. *Blood* 108(2):493–500.
19. Grenda DS, et al. (2007) Mutations of the ELA2 gene found in patients with severe congenital neutropenia induce the unfolded protein response and cellular apoptosis. *Blood* 110(13):4179–4187.
20. Pabst T, et al. (2001) AML1-ETO downregulates the granulocytic differentiation factor C/EBPalpha in t(8;21) myeloid leukemia. *Nat Med* 7(4):444–451.
21. Hirai H, et al. (2006) C/EBPbeta is required for 'emergency' granulopoiesis. *Nat Immunol* 7(7):732–739.
22. Bedi R, Du J, Sharma AK, Gomes I, Ackerman SJ (2009) Human C/EBP-ε activator and repressor isoforms differentially reprogram myeloid lineage commitment and differentiation. *Blood* 113(2):317–327.
23. Friedman AD (2007) Transcriptional control of granulocyte and monocyte development. *Oncogene* 26(47):6816–6828.
24. Hetz C (2012) The unfolded protein response: Controlling cell fate decisions under ER stress and beyond. *Nat Rev Mol Cell Biol* 13(2):89–102.
25. Skokowa J, et al. (2006) LEF-1 is crucial for neutrophil granulocytopoiesis and its expression is severely reduced in congenital neutropenia. *Nat Med* 12(10):1191–1197.
26. Mempel K, Pietsch T, Menzel T, Zeidler C, Welte K (1991) Increased serum levels of granulocyte colony-stimulating factor in patients with severe congenital neutropenia. *Blood* 77(9):1919–1922.
27. Nakahata T, Ogawa M (1982) Hemopoietic colony-forming cells in umbilical cord blood with extensive capability to generate mono- and multipotential hemopoietic progenitors. *J Clin Invest* 70(6):1324–1328.